PRODUCTION AND DECAY OF CHARMED PARTICLES IN e^+e^- COLLISIONS*

A. Barbaro-Galtieri

Lawrence Berkeley Laboratory
University of California
Berkeley, California 94720

ABSTRACT

This is a review of all the data available on production and decay of charmed particles in e^+e^- collisions. Production and decay of D^*, D, F mesons and charmed baryons are discussed. Comparisons with theoretical predictions, where available, are made.

TABLE OF CONTENTS

I. Introduction
II. Naive Quark Model Predictions for Charmed Particles
  A. Expected states with charm quantum number
  B. Hadron production in e^+e^- collisions
    1. Total hadronic cross section
    2. Vector meson formation
  C. Expected decays of charmed particles
    1. Four-quark case
    2. Six-quark case
    3. Nonleptonic enhancement
III. Production of Charmed Particles
  A. D and D* mesons
    1. Evidence for D and D* production
    2. Associated production of D and D*
    3. Inclusive D production cross section
  B. F Meson
  C. Charmed baryons
  D. Summary of contributions to R

* Lectures presented at the XVI International School of Subnuclear Physics, Erice, Italy, July 31-August 11, 1978.

EXB

IV. Properties of Charmed Mesons
A. Masses of D and D* mesons
1. D masses
2. D* masses
3. Charged-neutral D and D* mass differences
B. $D^0 - \bar{D}^0$ mixing
C. D* branching fractions
D. Decay properties of the D meson
1. Hadronic decay modes
2. Semileptonic decays
3. The nonleptonic enhancement question
4. D meson inclusive decays
5. Cabibbo forbidden decays
6. Summary of D decays

I. *INTRODUCTION*

Since the discovery of J/ψ in 1974, a lot of data has been accumulated on charmed particles. In these lectures I will review all that we have learned so far on charmed particles from e^+e^- collisions.

Section II will give naive quark model predictions on production and decays of charmed particles. In particular, the expectation for R, the total hadronic cross section divided by $\sigma_{\mu\mu}$, and for vector meson production will be discussed. Section III will deal with evidence for D, D*, F and charmed baryon production and their cross sections as well as with the resonant states above $c\bar{c}$ threshold. In Section IV all the results on masses of D and D* and decay properties of the D mesons will be presented and compared with expectation.

II. NAIVE QUARK MODEL PREDICTIONS FOR CHARMED PARTICLES

There are many excellent review articles on theoretical predictions for production and decay of charmed particles. Here, while discussing the experimental data, we will only review the most basic expectations of the quark model. For a more complete treatment of the subject we refer the reader, for example, to Refs. 1-3.

A. Expected States with Charm Quantum Number

With the addition of a fourth quark, charm, a number of new states are expected by combining it with the old quarks.

For the pseudoscalar mesons we can construct all the states shown in the following 4×4 matrix:

	$\bar{u}$	$\bar{d}$	$\bar{s}$	$\bar{c}$
u	$\frac{\eta' + \eta + \sqrt{2}\pi^0}{2}$	π^+	K^+	$\bar{D}^0$
d	π^-	$\frac{\eta' + \eta - \sqrt{2}\pi^0}{2}$	K^0	D^-
s	K^-	$\bar{K}^0$	$\frac{\eta' - \eta}{\sqrt{2}}$	F^-
c	D^0	D^+	F^+	η_c

that is, we add at least seven more pseudoscalars to the ones of the old spectroscopy. The new states are

$c\bar{u}$	D^0
$c\bar{d}$	D^+
$c\bar{s}$	F^+
$c\bar{c}$	η_c

and the charge conjugates of the first three. We also expect the vector mesons to increase by the same number, and so on for the other nonets. In addition to the η_c we expect to find an η_c', because the first excitation level of the $c\bar{c}$ system is expected to be very close in mass to the ground level. The same consideration is valid for the ψ. As we will see in Section II.B.2, many of these excitation states have been found (see Table I).

As for the baryons (qqq states) the increase is even more dramatic:

u d s		$\rightarrow$	u d s c
$(\frac{1}{2})^+$	octet	$\rightarrow$	20-plet
$(\frac{3}{2})^+$	decuplet	$\rightarrow$	20-plet

The $J^P = (\frac{1}{2})^+$ 20-plet is made of the old octet with $c = 0$, nine new states with $c = 1$, and three with $c = 2$. As for the 20-plet with

$J^P = (\frac{3}{2})^+$ we expect, in addition to the old decuplet, six states with c = 1, three with c = 2, and one with c = 3.

In these lectures we will talk about the production and properties of D and D* states and discuss the experimental evidence for F meson and charmed baryon production in e^+e^- annihilation.

B. Hadron Production in e^+e^- Collisions

Figure 1 shows some schematic diagrams of the major phenomena occurring in e^+e^- collisions at the presently available energies (total energy E < 10 GeV). Diagrams (a) and (b) represent the most

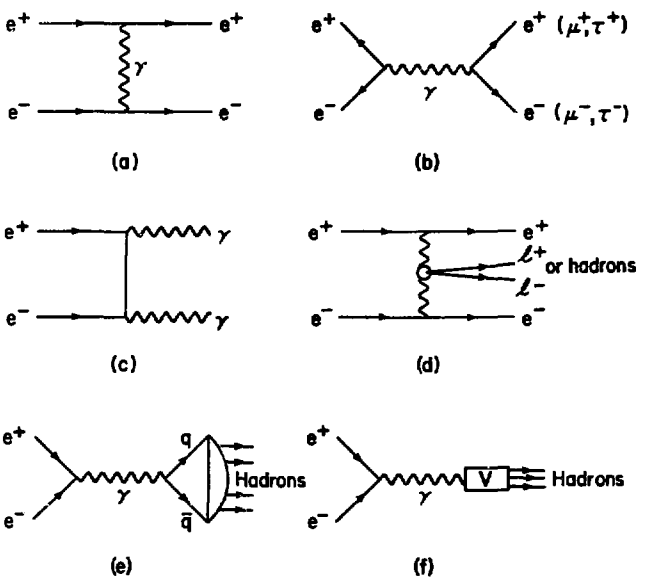

Fig. 1. Some schematic diagrams of processes taking place in e^+e^- collisions. The wavy lines represent the photon, the full lines are leptons and hadrons.

copious QED processes producing lepton pairs (the one photon processes); diagram (c) is one of the two possible diagrams for the annihilation into two photons; diagram (d) represents the so called "two photon" production, it only contributes a few percent of the hadronic cross section at these energies and will not be mentioned any further in these lectures. Finally, diagrams (e) and (f) represent the one photon hadron production and are the diagrams relevant to charmed particle production.

1. Total Hadronic Cross Section. The cross section for $q\bar{q}$ pair production can be calculated from QED, treating the quarks as point-like objects. In this case the cross section can be calculated in the same way as for a QED process involving leptons [diagram (b) in Fig. 1]. For μ pairs, at a total energy of $\sqrt{s}$, it is

$$\sigma_{\mu\mu} = \sigma(e^+e^- \to \mu^+\mu^-) = \frac{4\pi\alpha^2}{3s} = \frac{21.7}{E_b^2} \text{ nb} \qquad (1)$$

where E_b (in GeV) is the energy of one of the beams. The difference between diagrams (e) and (b) in Fig. 1 is that μ and q have different charges. The cross section for hadron production, assuming that the probability for $q\bar{q}$ pairs to go into hadrons is unity, is

$$\sigma_h = \sigma(e^+e^- \to \text{hadrons}) = \sigma_{\mu\mu} \cdot 3 \cdot \sum_i Q_i^2 \qquad (2)$$

where the $\sum_i$ includes the charges of all the types of quarks involved and the factor 3 comes from quantum chromodynamics (QCD), that is, from the hypothesis that quarks come in three colors. It is customary to analyze the experimental data in terms of

$$R = \frac{\sigma_h}{\sigma_{\mu\mu}} = 3 \sum Q_i^2 \qquad (3)$$

in order to be able to detect the deviation from this simple hypothesis. Of course, the expression (3) is not expected to be valid where resonant processes, like the diagram of Fig. 1(f), occur. We will discuss that case in the next section.

At low energies only u, d, and s quarks are involved. Away from resonances we expect

$$R = 3\left(\frac{1}{9} + \frac{1}{9} + \frac{4}{9}\right) = 2 \text{ , below charm threshold} \qquad (4a)$$

and

$$R = 3\left(\frac{1}{9} + \frac{1}{9} + \frac{4}{9} + \frac{4}{9}\right) = \frac{10}{3} \text{ , above charm threshold} \qquad (4b)$$

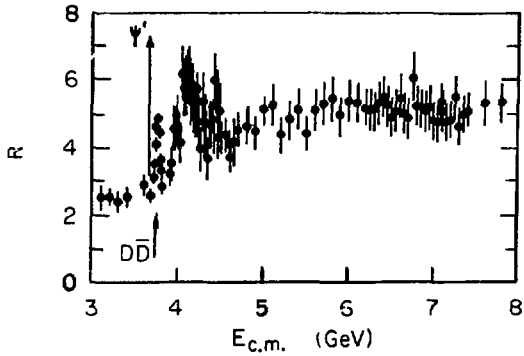

XBL 7912-13697

Fig. 2. The ratio of the total hadronic cross section to the μ pair production cross section, $R = \sigma_h/\sigma_{\mu\mu}$, as a function of the center of mass energy. The plot is taken from Ref. 4, the data[5] at the $\psi(3772)$ have been added to it.

Figure 2 shows the value of R measured at SPEAR in the 3 to 8 GeV energy regions.[4,5] Below and above charm threshold for the hadronic component of R, we find approximately

$$R_a = 2.5 \quad , \quad \text{below charm threshold}$$

$$R_b = 5.2 - 1 = 4.2 \, , \quad \text{above 6 GeV}$$

where we have subtracted one unit of R for heavy lepton production. In the region just above charm threshold resonance structures are present; we will discuss these in the next section.

In general, the total hadronic cross section behaves as expected for the onset of production of a new type of particle, as a simple quark counting model would predict. To check if particles with a new quantum number are produced and that, in fact, they correspond to the expectation from a charmed quark, we have to go into more details and study the different hadronic final states. This is the subject of these lectures.

The experimental values of R_a and R_b deviate from the naive quark model expectation [Eqs. (4a) and (4b)]. In QCD one would expect corrections due to quark-gluon interactions. Away from thresholds and resonant structures these corrections, in an

asymptotically free theory, have been estimated to give[6]

$$R = 3 \sum Q_i^2 \left(1 + \frac{\alpha_S(E)}{\pi}\right) \qquad (5)$$

where $\alpha_S(E)$, defined in analogy to α, the fine structure constant, is the running coupling constant of asymptotically free theories. In a particular $SU(4) \times SU(3)$ model with only four quarks, α_S has the form[7]

$$\alpha_S(E) = \frac{\alpha_S(E_o)}{1 + \frac{25}{12\pi} \alpha_S(E_o) \ln \frac{E}{E_o}} \quad . \qquad (6)$$

For a detailed review of these ideas, see Appelquist et al.[3] The experimental value of R differs from the expected value (Eq. 4) by about 25% above charm threshold, which would imply a value of $\alpha_S \sim 0.7$ in the 5-8 GeV region. This value of α_S is in gross disagreement with the value of $\alpha_S \sim 0.2$ evaluated at the ψ, as we will see in the next section. However, as discussed in Section III.D, the systematic errors on the measured R are quite large.

2. Vector Meson Formation. Close to a resonance in the $q\bar{q}$ system, the cross section (Eq. 2) has to be modified to account for the resonant matrix element. The cross section for vector meson production (diagram (f) in Fig. 1) and decay into the final state i, takes the form

$$\sigma(e^+e^- \to V \to i) = \frac{\pi(2J+1)}{s} \frac{\Gamma_e \Gamma_i}{(E-M)^2 + \Gamma^2/4} \qquad (7)$$

where M is the mass of the vector meson, Γ its total width, Γ_e and Γ_i the partial widths into electron pairs (the incoming channel) and into the i^{th} final state respectively. The factors of α and Q are now included in the partial widths, as we will see shortly. For vector mesons, that of course couple to the e^+e^- system through the photon [Fig. 1(f)], $J = 1$, so at resonance Eq. (7) becomes

$$(\sigma_0)_i^{max} = \frac{12\pi}{M^2} \frac{\Gamma_e \Gamma_i}{\Gamma^2} \qquad (8)$$

the subscript σ_0 has been added to remind the reader that this expression is valid only if radiative effects were not present. In order to compare with the data, radiative corrections have to be applied either to the formula or to the data. These corrections have been discussed in the literature[8] and summarized recently by

Jackson and Scharre.[9] In addition to radiative corrections, often the uncertainty in the energy of the e^+e^- beams contributes to alter the resonant shape (Eq. 7) and has to be taken into account, especially when Γ is small compared with the beam resolution. Techniques used to take into account these effects are extensively described in Ref. 9. Because of these corrections the relevant measurement is the area of the resonance curve instead of the height. For the cross section in the i^{th} final state we have:

$$\int \sigma_i \, dE = (\text{Area})_o^i = \pi \frac{\Gamma}{2} (\sigma_o)_i^{max}$$

so it is

$$\frac{\Gamma_e \Gamma_i}{\Gamma} = \frac{M^2}{6\pi^2} \int \sigma_i \, dE \quad . \tag{9}$$

Through this expression and similar ones for the different final states we can determine experimentally Γ_e, Γ_i, and the total width $\Gamma = \sum_i \Gamma_i$.

The vector mesons produced in e^+e^- interactions in the 2-8 GeV energy region appear as peaks in a plot of R (Fig. 2). In Table I we tabulate some parameters for the vector mesons of the new spectroscopy (states of $c\bar{c}$) and the ρ, ω, and ϕ of the old spectroscopy. For completeness we have added the T and T' recently observed at high energies,[10-12] they are $b\bar{b}$ bound states (b is the bottom quark of charge $Q = -1/3$). For a discussion of the relation between Γ_e and the charge of the quark responsible for the T and T' as well as for a discussion of different choices of potential to describe $q\bar{q}$ systems, see Quigg and Rosner.[13] The states of $c\bar{c}$ above ψ and ψ' are above threshold for charmed particle production and will be discussed in Section III.A.2. Note that

$$M_{\psi'} - M_{\psi} = 589 \pm 1 \text{ MeV}$$

$$M_{T'} - M_{T} = 556 \pm 3 \text{ MeV}$$

as quoted in Ref. 16 and 20 respectively. These mass differences are relevant to the choice of a potential to describe the $q\bar{q}$ system.[3,13]

The theoretical expressions for Γ_e and the other partial widths depend upon the model used to calculate them. In general for a $q\bar{q}$ bound state going into e^+e^- as in the diagram at right, the

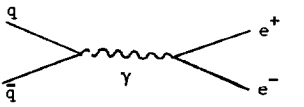

TABLE I. Resonance parameters for vector mesons.[a] Γ is the total width, Γ_e is the partial width to electron pairs, and B_e is the branching fraction to electron pairs.

State	Mass (MeV)	Γ (MeV)	Γ_e (keV)	B_e	Ref.
ρ	776±3	155±3	6.7 ±0.8	$(4.3\pm0.5)10^{-5}$	14
ω	782.6±0.3	10.1±0.3	0.76±0.17	$(7.6\pm1.7)10^{-5}$	14
ϕ	1019.6±0.2	4.1±0.2	1.31±0.10	$(31\pm1)10^{-5}$	14
ψ	3095±4	0.069±0.015	4.8 ±0.6	$(69\pm9)10^{-3}$	SLAC-LBL[15]
ψ'	3684±5	0.228±0.056	2.1 ±0.3	$(9.3\pm1.6)10^{-3}$	SLAC-LBL[16]
ψ''	3772±6	28 ±5	0.35±0.09	$(1.2\pm0.3)10^{-5}$	Rapidis et al.[5]
	3770±6	24 ±5	0.18±0.06	$(0.7\pm0.2)10^{-5}$	DELCO[17]
4.04[b]	4040±10	52 ±10	0.75±0.10	$(1.4\pm0.4)10^{-5}$	DASP[18]
4.16[b]	4159±20	78 ±10	0.77±0.20	$(0.9\pm0.3)10^{-5}$	DASP[18]
4.41	4414±7	33 ±10	0.44±0.14	$(1.3\pm0.3)10^{-5}$	SLAC-LBL[19]
T	9460±10	~0.05	1.2 ±0.2	$(2.6\pm1.4)10^{-2}$	20[c]
T'	10016±10	--	0.33±0.10	--	20[c]

[a] Other states have been reported between the ϕ and the ψ by experiments at Frascati and Orsay; we do not include them here.

[b] The SLAC-LBL and DELCO data do not separate this region into two states (see Figs. 2 and 14).

[c] Values for T and T' are averages as quoted by Flügge.[20]

leptonic width has been calculated to be[21]

$$\Gamma_e = \frac{16\pi \alpha^2 Q^2}{M^2} |\psi(0)|^2 \qquad (10)$$

where M is the mass of the vector meson, Q the charge of the quark and $|\psi(0)|^2$ is the square of the wave function at the origin and it depends upon the potential chosen to represent the $q\bar{q}$ interaction. Extensive work has been done to understand the $c\bar{c}$ interactions. Appelquist and Politzer[22] conjectured the existence of $c\bar{c}$ bound states, that is, states below the threshold for producing particles with charm, just about at the same time that the ψ was discovered.[23]

Eichten et al[24] have used a short range Coulomb potential and a long range linear potential to describe $c\bar{c}$ interactions and have been successful in predicting some of the features of the charmonium spectrum, including the existence of $\psi''(3772)$, later discovered.[5] The experimental data on charmonium spectroscopy are discussed in Prof. Wolf's lectures and will not be discussed here. For a review of the theoretical work on charmonium see Refs. 1, 3 and 25, where expressions for Γ_h can be found. We will only discuss here briefly Γ_h for the ψ, as derived by Appelquist and Politzer.[22] The $\psi \to h$ process (for $\psi \to 3\pi$ a schematic diagram is shown in Fig. 3c) can take place through three-gluon exchange. In analogy with the three-gamma process in positronium, by substituting α^3 with $5/18\ \alpha_S^3$, they derived the expression

$$\Gamma(\psi \to h) = \frac{40}{81\pi} (\pi^2 - 9) \frac{\alpha_S^3}{M^2} |R(0)|^2 \qquad (11)$$

where $|R(0)|^2 = 4\pi |\psi(0)|^2$. By measuring Γ_e and Γ_h (see Table I) and using Eqs. (10) and (11), one can calculate the value for α_S at the ψ to be

$$\alpha_S(3.1) = 0.19 \quad . \qquad (12)$$

We comment here that charmonium models using a more sophisticated potential than that of Ref. 24 require $\alpha_S \sim 0.4 - 0.5$ to fit the charmonium spectrum. We refer the reader to Ref. 3 and 81 for discussion of this point.

One final observation on the parameters of Table I is with regard to total widths. The ψ and ψ' that are $c\bar{c}$ bound states, and Υ and Υ' that are $b\bar{b}$ bound states, have a very narrow total width. This is expected by the OZI rule,[26] found empirically years ago to explain the observed rates in meson decays. This rule says that transitions described by diagrams where the initial

quarks annihilate each other and do not appear in the final state are suppressed. The relevant diagrams for ϕ, ψ and ψ'' decays are shown in Fig. 3. Diagrams (a) and (c) are forbidden by the OZI rule, diagrams (b) and (d) are allowed. For the ϕ decay, the ratio of rates for diagrams (b) and (a) is not very large due to kinematic factors. There are various possible dynamical approaches to the theoretical understanding of the OZI rule, but a quantitative formulation of this rule has not been achieved yet. See Jackson's review of this point.[1] In any case, the OZI rule tells us that above threshold for $D\bar{D}$ production we should expect Γ_{tot} to be larger than those observed for ψ and ψ', which is what we see in Table I.

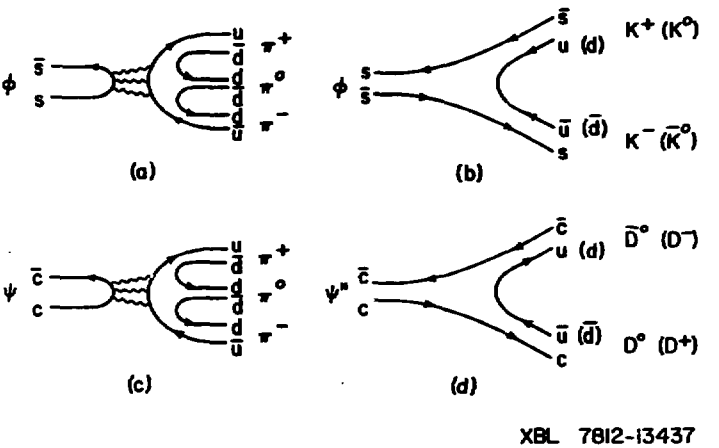

Fig. 3. Illustration of the OZI rule. Diagrams (a) and (c) are forbidden, (b) and (d) are allowed. The decay rates for the four diagrams are $\Gamma_a = 0.6$ MeV, $\Gamma_b = 3.4$ MeV, $\Gamma_c = 0.7$ keV, and $\Gamma_d = 28$ MeV. The wavy lines represent gluons.

C. Expected Decays of Charmed Particles

The charmed quark, c, was introduced by Glashow, Iliopoulos and Maiani (GIM)[27] to explain the absence of strangeness changing neutral currents; that is, the nonobservation of decays like $K^0 \to \mu^+\mu^-$ (now measured to have a branching fraction of 9×10^{-9}) and $K^- \to \pi^-\nu\bar{\nu}$. The presence of a fourth quark would produce the cancellation of the $\Delta S = 1$ piece of the neutral current.

The expected decays of charmed particles can be derived using a conventional Weinberg and Salam theory[28] with left-handed weak isodoublets and right-handed weak isosinglets, along with the GIM quark structure.[27] One possible model with six leptons and six quarks (see for example the review of Harari on a variety of possible models[2]) includes the following isodoublets:

$$\begin{pmatrix}\nu_e\\ e^-\end{pmatrix}_L \begin{pmatrix}\nu_\mu\\ \mu^-\end{pmatrix}_L \begin{pmatrix}\nu_\tau\\ \tau^-\end{pmatrix}_L \qquad \begin{pmatrix}u\\ d'\end{pmatrix}_L \begin{pmatrix}c\\ s'\end{pmatrix}_L \begin{pmatrix}t\\ b\end{pmatrix}_L \tag{13}$$

where

$$\begin{aligned} d' &= d\cos\theta + s\sin\theta \\ s' &= -d\sin\theta + s\cos\theta \end{aligned} \tag{14}$$

with θ the Cabibbo angle[29] introduced in 1963 to explain the decay properties of mesons and baryons made up of u, d and s quarks. Here we have included the τ heavy lepton, established as a new particle and very likely to be a sequential heavy lepton,[30] and a new quark doublet of which only the bottom one, b, has been observed (see Section II.B.2).

1. The Four Quark Case. Let us just consider four quarks first. The decay characteristic of charmed particles are dictated from whatever charged current we can form in this framework. The charged current has the form:

$$J_h^c = \bar{u}d' + \bar{c}s' = \bar{u}(d\cos\theta + s\sin\theta) + \bar{c}(s\cos\theta - d\sin\theta)$$

which can also be written as

$$J_h^c = \cos\theta\,(\bar{u}d + \bar{c}s) + \sin\theta\,(\bar{u}s - \bar{c}d) \tag{15}$$

where the quark symbols have been used instead of the complete expression for the current, i.e., $\bar{u}d = \bar{u}\gamma_\mu(1-\gamma_5)d$. The values of the coefficients are $\cos\theta = 0.974$ and $\sin\theta = 0.227$, and for this reason the transitions that can be done with the first term

of the current are called "Cabibbo favored" and the others are called "Cabibbo suppressed."

The "favored" decays of the c quark are the transitions with

$$c \to s \ , \quad \text{with} \quad \Delta C = \Delta S = \Delta Q \ , \quad \Delta I = 0 \ , \tag{16}$$

the "Cabibbo suppressed" are the transitions

$$c \to d \ , \quad \text{with} \quad \Delta C = \Delta Q \ , \quad \Delta S = 0 \ , \quad \Delta I = \tfrac{1}{2} \ . \tag{17}$$

Some diagrams for two-body Cabibbo-favored and Cabibbo-suppressed modes of the charmed mesons are shown in Fig. 4. Notice that in order to have a "Cabibbo favored" decay of these mesons, the c quark has to decay according to (16) and the W must have the favored transition $W \to u\bar{d}$ as in Eq. (15). From these diagrams (just on the basis of diagram counting) we notice that:

a. Diagrams of type (b) are nine times more likely than diagrams like (d), because in (b) the $u\bar{d}$ pair can have any of three colors, whereas in (d) the $u\bar{d}$ pair must have the same color as c and $\bar{s}$.

b. Comparing (a) and (c) one can easily derive that (a) is a factor 3 larger because of the three colors of the quarks. Here we comment that on the basis of diagram counting we would expect

$$\begin{aligned} D^0 &\to K^- + \text{hadrons} && 50\% \\ D^0 &\to K^- + e^+ + \ldots && 20\% \\ D^0 &\to K^- + \mu^+ + \ldots && 20\% \end{aligned} \tag{18}$$

We will come back to this point in Section 3 below.

c. The rates for the "Cabibbo suppressed" decays are smaller than the "favored" ones by at least a $\tan^2\theta = 0.55$ factor. Of course, phase space factors are to be properly taken into account.

In summary, just on the basis of the predictions of Eqs. (15) (16) and (17), we would expect that charmed mesons prefer the following hadronic decays:

$$\begin{aligned} D^0 &\to K^-\pi^+, \ \bar{K}^0\pi^0, \ \bar{K}^0\pi^+\pi^-, \ \bar{K}^0\eta, \ \bar{K}^0\eta', \ \text{etc.} \\ D^+ &\to \bar{K}^0\pi^+, \ K^-\pi^+\pi^+, \ \text{etc.} \\ F^+ &\to \bar{K}^0K^+, \ K^+K^-\pi^+, \ \eta\pi^+, \ \eta'\pi^+, \ \text{etc.} \end{aligned}$$

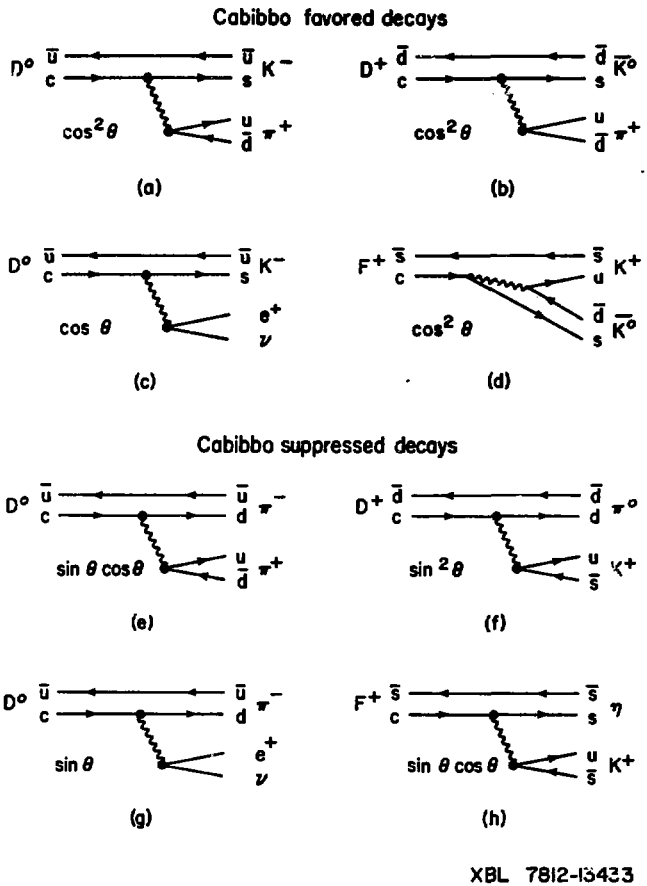

XBL 7812-13433

Fig. 4. Schematic diagrams illustrating charmed particle decays. The wavy lines represent the W boson, solid lines are hadrons or leptons. Diagrams (a)-(d) are for Cabibbo favored decays, (e)-(h) are for Cabibbo suppressed decays. The amplitude for each diagram is proportional to cosθ or sinθ factors as shown.

and the following semileptonic decays:

$$D^0 \to K^- e^+ \nu, \quad K^{*-} e^+ \nu, \quad K^- \mu^+ \nu, \quad \text{etc.}$$

$$D^+ \to \bar{K}^0 e^+ \nu, \quad \bar{K}^{*0} e^+ \nu, \quad \text{etc.}$$

$$F^+ \to \eta e^+ \nu, \quad \eta' e^+ \nu, \quad \text{etc.}$$

2. The Six Quark Case. If we introduce mixing of d, s and b quarks we need three angles and a phase to describe such mixing.[31] This means that instead of a 2×2 matrix as in Eq. (14), we have a 3×3 unitary matrix.

$$J_h^c = \bar{u}\,\bar{c}\,\bar{t}\,\gamma_\mu(1-\gamma_5)U \begin{pmatrix} d \\ s \\ b \end{pmatrix}$$

$$U = \begin{pmatrix} C_1 & -S_1C_3 & -S_1S_3 \\ S_1C_2 & C_1C_2C_3 - S_2S_3\, e^{i\delta} & C_1C_2S_3 + S_2C_3\, e^{i\delta} \\ S_1S_2 & C_1S_2C_3 + C_2S_3\, e^{i\delta} & C_1S_2S_3 - C_2C_3\, e^{i\delta} \end{pmatrix} \quad (19)$$

where $C_i = \cos\theta_i$, $\quad i = 1,2,3$

$S_i = \sin\theta_i$.

In a graphic presentation Fig. 5 shows how the transition from one quark to another can be calculated for the two different cases: d-s and d-s-b mixing.

In Eq. (19), θ_1 is the original Cabibbo angle. As for the others, one can try to calculate the upper limits for θ_2 and θ_3 by using some decay modes or other phenomena involving old quarks (see for example, Harari's review[2]).

a. From $u \to d$, in $n \to p e^- \nu$ one finds

$|\cos\theta_1| = 0.974 \pm 0.002$, $|\theta_1| = (13.2 \pm 0.5)^\circ$, $(|S_1| = 0.227)$.

b. From $u \to s$, in $\Lambda \to p e^- \nu$ or $K \to \pi e \nu$, the latest fits[84] give

$\sin\theta_1 \cos\theta_3 = 0.219 \pm 0.011$, or $S_3 = 0.28^{+0.21}_{-0.28}$

which gives

$|\cos\theta_3| > 0.87 \qquad |\theta_3| < 29^\circ$, $\qquad (|S_3| < 0.49)$.

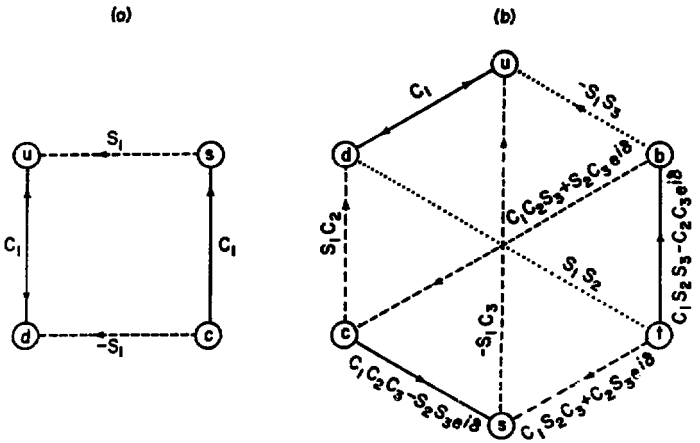

XBL 7812-13435

Fig. 5. Graphic representation of transitions between quarks. Solid lines represent the most copious transitions (only $\cos\theta_i$ factors), dashed lines are for transitions with a $\sin\theta_i$ factor, and the dotted lines have two $\sin\theta_i$ factors. (a) is for the four quark case, (b) is for the six quark case.

c. From K_S-K_L mass difference,[32] we get the limit (for $m_c = 1.55$ GeV, $m_t > 5$ GeV),

$$\tan^2\theta_2 < m_c/m_t \quad \text{or} \quad |\theta_2| < 30^\circ \qquad (|s_2| < 0.5).$$

d. Not very much can be said about δ, which is related to CP violation.[33] The only statement one can make at this time from CP violation parameters in $K^0 \to 2\pi$, is that

$$\sin\delta > 5\times10^{-3} \quad \text{or} \quad \delta > 0.3^\circ .$$

In conclusion, since θ_2, θ_3 are small, Eq. (19) tells us that the basic content of (15) ($c \to s$ is the favored decay and $c \to d$ is the suppressed decay) still holds for the charmed quark.

3. Nonleptonic Enhancement. With the assumption that the W couples equally to quark or lepton pairs, we would expect, as mentioned in section 1, that the inclusive semi-leptonic decays into e and μ would be about 40%, as from Eq. (18). Does this diagram counting rule work for strange particle decays? The answer is no.

The nonleptonic decay rates of strange particles, both mesons and baryons, are found to be larger than expected. Specifically, the amplitude for the $\Delta I = 1/2$ part of the nonleptonic interaction is enhanced by about a factor of 20 over the $\Delta I = 3/2$ part of the nonleptonic amplitude and the semileptonic amplitude. For example:

$$(K_S \to \pi^+\pi^-) = 0.77 \times 10^{10} \text{ sec}^{-1}, \quad \Delta I = 1/2, 3/2$$

$$(K^+ \to \pi^+\pi^0) = 0.17 \times 10^{8} \text{ sec}^{-1}, \quad \Delta I = 3/2$$

the $K^+ \to \pi^+\pi^0$ decay rate is much smaller than the first one, as the $\Delta I = 1/2$ enhancement would predict. For a discussion of the experimental evidence for the $\Delta I = 1/2$ rule in K meson and hyperon decays, see the Appendices of the Particle Data Group compilation.[14] Since the $\Delta I = 1/2$ part of the transition appears alone in the octet part of the Hamiltonian, this experimental observation has been called "octet enhancement." As for a dynamical mechanism that would produce such an enhancement, it has been suggested that it could arise from the strong interactions among the constituents at short distance.[34]

What do we expect for charmed particles? Although the mechanism that produces octet enhancement is not fully understood, the same phenomenon has been extended to charmed particle decays by various authors.[35,36] Einhorn and Quigg[37] worked out the necessary group theory for extending the SU(3) phenomenon to SU(4) and concluded that octet enhancement results in 20-plet enhancement for the four-quark case. For SU(3) the weak Hamiltonian reduces to the following representations

$$H_W = \underline{1} \oplus \underline{8} \oplus \underline{27} \tag{20}$$

Here since the $\underline{8}$ representation contains only the $\Delta I = 1/2$ transition, the octet part is found to be the most important one. For the SU(4) case the weak Hamiltonian reduces[37] to

$$H_W = \underline{20} \oplus \underline{84} \tag{21}$$

and by further dividing these two representations into their SU(3) components they conclude that the $\underline{20}$ part will be enhanced.

How large is this enhancement? The predictions differ; for

example, the decay $D^+ \to \bar{K}^o\pi^+$ would be completely forbidden for some authors,[37] allowed for others. Ellis et al[38] predict $\Gamma(D^+ \to \bar{K}^o\pi^+) \sim \Gamma(D^o \to K^-\pi^+)$. As for the semileptonic decays the predictions vary also, the $D \to e$ inclusive rate could be as low as 3% of the total rate according to Ellis et al.[38] So the extreme case gives

$$\begin{aligned} D^o &\to K^- + \text{hadrons} \quad 94\% \\ D^o &\to K^- + e^+ + \ldots \quad 3\% \\ D^o &\to K^- + \mu^+ + \ldots \quad 3\% \end{aligned} \tag{22}$$

This has to be compared with the quark diagrams counting case (Eq. 18). It is interesting to compare the experimental results with these two cases. It is clear that only the data will shed some light on the magnitude of the nonleptonic enhancement. We will return to this point in Section IV.D when we will discuss our experimental results.

III. PRODUCTION OF CHARMED PARTICLES

Most of the results discussed in these lectures have been obtained with the SLAC-LBL magnetic detector Mark I. I will refer to two different experiments done with this detector: the earlier SP17 experiment with the detector configuration described in Ref. 39 and the more recent SP26 experiment with a lead-glass array to detect γ and electrons.[40] This last experiment will be called the LGW. The detector in its last configuration is shown in Fig. 6. For details, the reader is referred to Refs. 39 and 40.

In this section we will discuss the evidence for production of charmed mesons and baryons in e^+e^- collisions, as well as the cross sections for production of these states. We will also relate these production rates to the total hadronic cross section.

A. D and D* Mesons

1. Evidence for D and D* Production. The total hadronic cross section normalized to $\sigma_{\mu\mu}$, R in Fig. 2, exhibits a rise with some resonance-like peaks just above the ψ' resonance. The data in the energy region $3.6 < E < 4.6$ GeV are shown in more detail in Fig. 7, taken from the paper of Rapidis et al.[5] The data in this energy region have provided all of the information we have on D and D* mesons: the D and D* have been discovered in the 4.03 and 4.4 GeV regions. Precise masses and D branching ratios have been measured at the 3.772 GeV resonance, the most recently discovered state of $c\bar{c}$.[5]

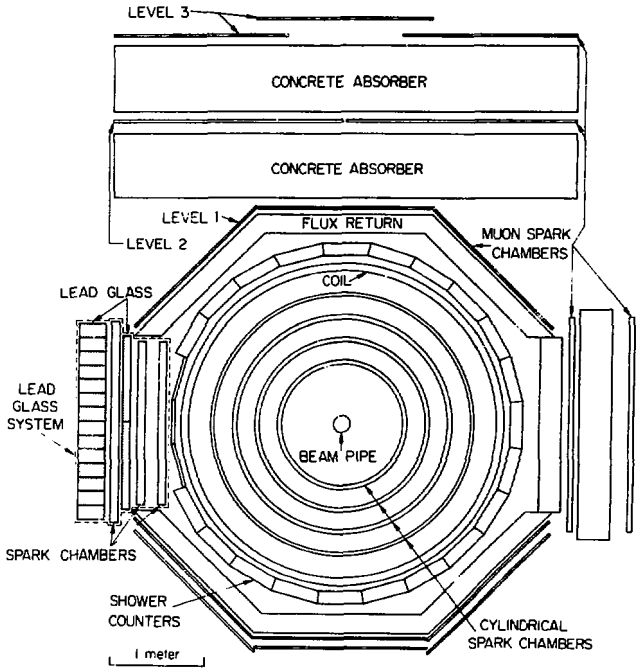

Fig. 6. The SPEAR magnetic detector[39] as seen looking along the beam line. The proportional chambers around the beam pipe and the trigger counters are not shown. The lead glass system (LGW)[40] is shown on the left side of the figure.

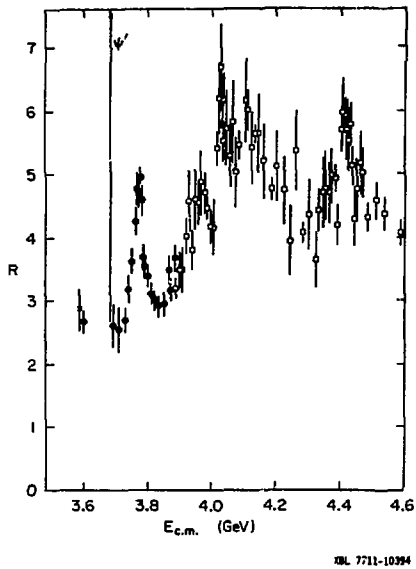

Fig. 7. R, the total hadronic cross section divided by $\sigma_{\mu\mu}$ versus $E_{c.m.}$. The full dots are the data of Rapidis et al.,[5] the squares are from Siegrist et al.[19] Radiative corrections have been applied.

The first direct evidence for charmed particle production has been reported by Goldhaber et al[41] in the invariant mass of the $K^{\mp}\pi^{\pm}$ system (D^{o}, $\bar{D}^{o}$) and shortly after by Peruzzi et al[42] in the invariant mass of the $K^{\mp}\pi^{\pm}\pi^{\pm}$ system ($D^{\pm}$). These results come from the SP17 experiment and are summarized in Fig. 8, taken from Piccolo et al.[43] The charged K's are identified by the time-of-flight measurement for a 1.5 - 2.0 meter flight path in the magnetic detector (the resolution is σ = 0.4 nsec). The neutral kaons are identified by measurement of the dipion mass and by requiring consistency of the dipion vertex with the direction of the kaon momentum.[44]

The following reactions and their charge conjugates are observed:

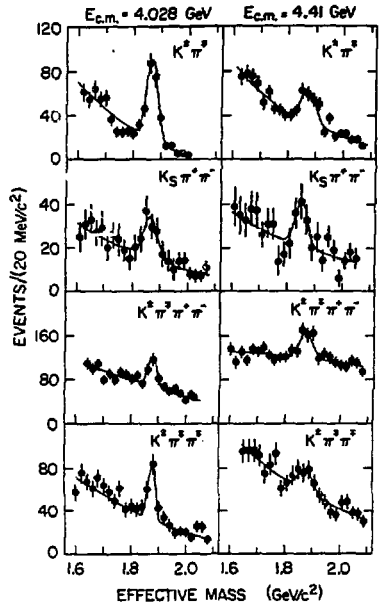

Fig. 8. Invariant mass distribution for various channels showing D^0 and D^+ signals. The data is that of Piccolo et al[43] at 4.03 and 4.41 GeV total e^+e^- energy.

$$e^+e^- \rightarrow D^0 + \text{recoil}, \quad \text{with} \quad D^0 \rightarrow K^-\pi^+ \tag{23}$$

$$D^0 \rightarrow K_S\pi^+\pi^- \tag{24}$$

$$D^0 \rightarrow K^-\pi^+\pi^+\pi^- \tag{25}$$

$$e^+e^- \rightarrow D^+ + \text{recoil}, \quad \text{with} \quad D^+ \rightarrow K^-\pi^+\pi^+ \tag{26}$$

The widths of the peaks observed are consistent with the experimental mass resolution of 20 MeV for the $K\pi$ system and 15 MeV for the $K^-\pi^+\pi^+$ system. In addition, the $K^-\pi^+\pi^+$ final state is exotic because the overall charge of the state (+) has the opposite sign from the strangeness of the state (-). These facts point clearly toward exclusion of a K* interpretation for this state. As a result of a fit[45] described in Section IV.C, the masses are found to be $M_0 = 1863 \pm 3$ MeV and $M_+ = 1874 \pm 5$ MeV. The most recent mass measurements, as well as more decay modes and absolute

branching ratios determined at the $\psi(3772)$, will be discussed in Section IV.

The D^{*0} and D^{*+} are also observed in these data as peaks in the mass of the recoil in reactions (23-26). For these reactions,

$$M^2_{recoil} = (E_{CM} - \sqrt{p^2 + M^2})^2 - p^2 \qquad (27)$$

where M and p are mass and momentum of the D. The resolution of M_{recoil} can be improved considerably by using the fixed values for the D^+ or D^0 masses determined above. Then there is a one to one correspondence between the recoil mass and the D momentum. The distribution of the recoil mass for reaction (23) at 4.03 GeV total E_{CM} energy is shown in Fig. 9. Two peaks are observed, the lower

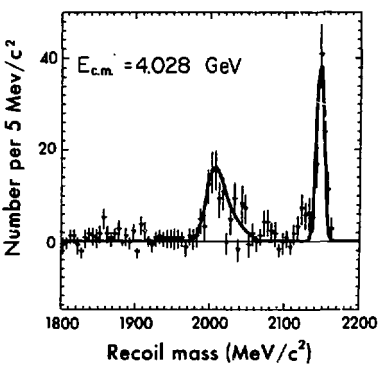

Fig. 9. The mass of the system recoiling against the D^0 in e^+e^- interactions at 4.03 GeV. Data are from Goldhaber et al.[45]

one at a mass of 2.01 GeV, the higher one at 2.15 GeV. They are interpreted as due respectively to the reactions

$$e^+e^- \rightarrow D^0 \bar{D}^{*0} \quad \text{(and complex conjugate)} \tag{28}$$

$$e^+e^- \rightarrow D^{*0} \bar{D}^{*0} \tag{29}$$

The Q of the first reaction (28) is 159 MeV, which results in a momentum for the directly produced D^0, p_D, of ~580 MeV/c. Because of this large value the uncertainty on p_D contributes considerably to the uncertainty on the recoil mass (see Eq. 27). The widening of the peak is also due to the fact that the observed D^0 can be from (a) direct D^0 produced, or (b) D^0 from the decays $D^{*0} \rightarrow D^0\gamma$ or $D^{*0} \rightarrow D^0\pi^0$, or (c) D^0 from the reaction $e^+e^- \rightarrow D^+D^{*-}$ with $D^{*-} \rightarrow D^0\pi^-$. For the second peak, the $D^{*0}\bar{D}^{*0}$ reaction has a small Q (Q = 16 MeV), therefore a smaller p_D that results in a narrower peak. More details on fitting these data to get D^* masses and branching ratios will be given in Section IV.

Before leaving the subject I want to remind you that the only other report of D production for which a peak is seen in an invariant mass distribution is by Baltay et al.[46] This is a Fermilab neutrino experiment in a bubble chamber filled with a heavy mix of hydrogen and neon. The channel observed is $D^0 \rightarrow K^0_S\pi^+\pi^-$.

2. Associated Production of D and D*. Above threshold for the reactions

$$e^+e^- \rightarrow D^0\bar{D}^0 \tag{30}$$

$$e^+e^- \rightarrow D^+D^- \tag{31}$$

associated production of a pair of charmed particles can occur. The $c\bar{c}$ model of Eichten et al[24] predicts resonant states of $c\bar{c}$ above charm threshold, besides the charmonium levels below it. Decays of these states into a pair of charmed particles are allowed by the OZI rule. Therefore, we expect their total widths to be much larger than those of the ψ and ψ' (see Section II.B.2, Table I and Fig. 7).

Eichten et al[47] have extended their $c\bar{c}$ model to these types of decays, and as we will see, can predict some of their properties.

The $\psi(3772)$, ψ'', is the first of such resonances above threshold. Figure 10 shows the detailed shape of R in this energy region as measured by the LGW experiment.[5] Figure 10a shows the raw data, whereas Fig. 10b shows the data after subtraction of the ψ' rapidly descending tail. This is due to the Gaussian resolution of the beam of 1 MeV, much wider than the ψ' width (see Table I) and to radiative effects. Both these corrections have been applied

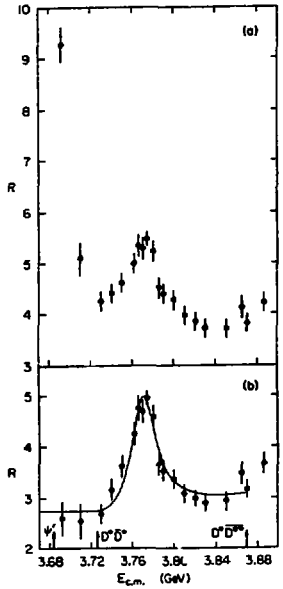

XBL 7711-10395

Fig. 10. R versus $E_{c.m.}$ at the $\psi(3772)$. (a) before, and (b) after radiative corrections and ψ' tail subtraction. The curve is a p-wave Breit-Wigner fit to the data.

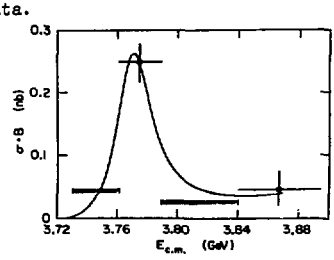

XBL 7711-10396

Fig. 11. Data[53] of $\sigma \cdot B$ versus $E_{c.m.}$ for D^0 and $\bar{D}^0$ decays into $K^{\mp}\pi^{\pm}$. The cross-hatched bars represent upper limits. The curve is the same one shown in Fig. 10 normalized to the 3.77 GeV point.

in Fig. 10b. The curve is a p-wave Breit-Wigner resonant shape. Figure 11 shows evidence that the decay $\psi'' \to D^0\bar{D}^0$ does in fact take place.[53] The cross section times B, the branching ratio for $D^0 \to K^-\pi^+$, is plotted versus the e^+e^- total energy. The curve is the same one of Fig. 10, normalized to the highest point.

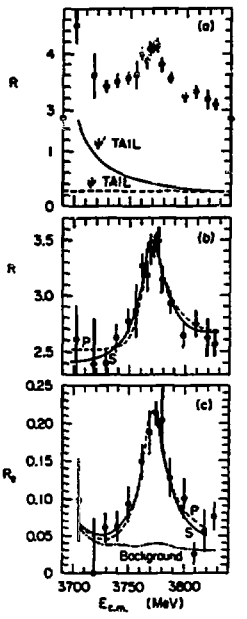

Fig. 12. R as a function of energy as measured by the DELCO experiment[17] at the $\psi(3772)$. (a) is the raw data; (b) the data after radiative correction and subtraction of the ψ' tail; (c) R for events with one electron or more in the final state. The curves are p-wave Breit-Wigner forms.

Figure 12 shows the data of the DELCO experiment[17] in the same energy region. The parameters shown in Table I are derived from Figs. 10 and 12.

The ψ'' is a $^3D_1$ state which is not expected to couple directly to the photon if we use the expression in Section II (Eq. 10) for Γ_e, because for a p-wave the wave function at the origin is zero. However, other effects[82] can produce coupling of the ψ'' to the e^+e^- system, the larger one being mixing with the nearby ψ'. The prediction of the $c\bar{c}$ model[47] for the Γ_e (Γ_e = 150 eV) is closer to the DELCO result[17] (see Table I). The ψ'' is expected to decay almost entirely into $D\bar{D}$, since $D\bar{D}^*$ is not energetically allowed.

No upper limits for the OZI forbidden decay modes are available experimentally.

The 3.95 GeV region. As we go to higher energy in Fig. 7, D and D* associated production is possible. There is a flattening off of the rise in R at about 3.95 GeV, but none of the experiments that measured the total cross section can clearly see a resonant state at this mass. For comparison, the measurements of DASP[18] and PLUTO[50] are shown in Fig. 13, taken from Ref. 18, and the data of DELCO[48] are shown in Fig. 14.

At 4.03 GeV a very striking peak is observed. This is associated with the threshold for $D^*\bar{D}^*$ associated production. As already discussed, Goldhaber et al[45] have studied in detail the composition of this bump and quote a ratio of cross sections for $D\bar{D}$, $D\bar{D}^*$ and $\bar{D}D^*$, and $D^*\bar{D}^*$ associated production. These values are shown in Table II along with the predictions of the charmonium model.[24,47] The $D^*\bar{D}^*$ production is very large if the kinematical factors are taken into account; in fact, phase space factors of p^3 certainly favor $D\bar{D}$ and $D\bar{D}^*$ or $\bar{D}D^*$. The ratios of R shown in the last line of Table II are spin factors, which predict a smaller $D^*\bar{D}^*$ production than the observed one. This fact prompted De Rujula et al[49] to interpret the $\psi(4.03)$ as a molecule, that is, a bound state of $D^*\bar{D}^*$. However, there is no detailed model for this hypothesis.

Above 4.03 GeV the data of Fig. 7 show a new resonant structure at 4.41 GeV, whereas the data of DASP[18] and PLUTO,[50] shown in Fig. 13, have an additional structure at 4.16 GeV. This is not observed clearly in either MARK I data[4] or DELCO data[48] at SPEAR, Fig. 14. At 4.4 GeV the detailed study of production of the different charmed particles is more difficult than at 4.03 GeV (the K identification gets worse with K momentum) and has not been done. As for the $c\bar{c}$ model the present calculations are not considered reliable[25] above 4.1 GeV and therefore their predictions should not be compared with the data.

3. Inclusive D Production Cross Section. The Lead-Glass Wall (LGW) experiment[51,52] has measured the inclusive D production cross sections in the 3.7 to 7.0 GeV energy region. The results are shown in Table III. Note that the D^+ cross section is systematically lower than the D^0 cross section. The last column of the table shows $R_{D\bar{D}}$ defined as

$$R_{D\bar{D}} = \frac{\sigma_{D^+} + \sigma_{D^0}}{2\sigma_{\mu\mu}} \qquad (32)$$

the factor 2 enters into this expression because it is assumed that a D and a $\bar{D}$ are produced in association, either directly or

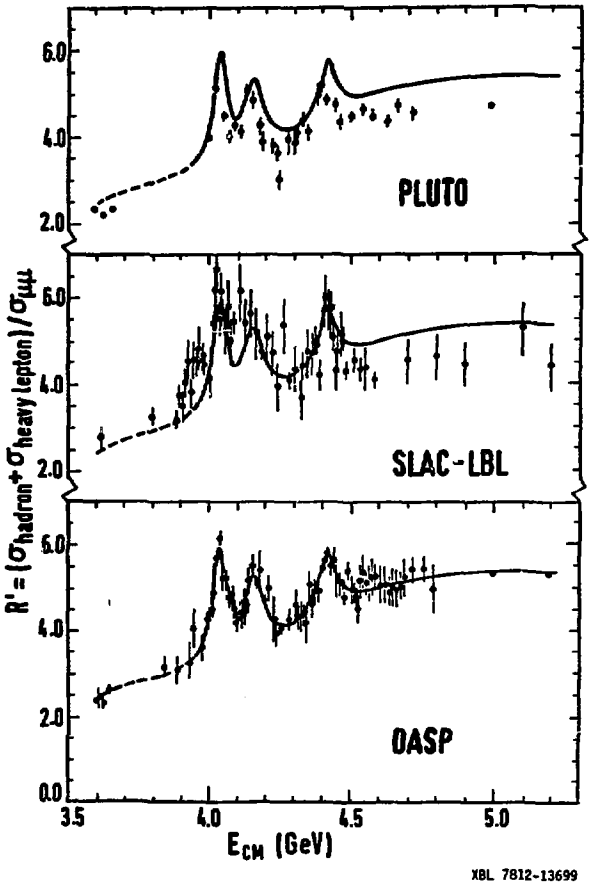

Fig. 13. R as a function of energy taken from the DASP paper of Brandelik et al.[18] The bottom graph shows the DASP data with a fitted curve; the other two graphs show the SLAC-LBL data[4] and the PLUTO data[50] compared with the DASP curve.

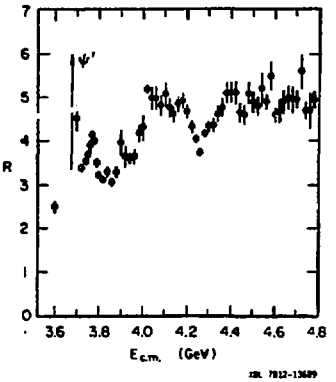

Fig. 14. R as a function of energy measured by the DELCO detector.[48]

TABLE II. Ratio of $R = \sigma_h/\sigma_{\mu\mu}$ for different associated charm production processes at the $\psi(4.03)$. For the values in the third line, the p^3 phase space factors have been explicitly removed.

$R(D\bar{D})$:	$R(D\bar{D}^* + \bar{D}D^*)$:	$R(D^*\bar{D}^*)$	Reference
0.10 ±0.06	0.85 ±0.09	1.00 ±0.10	Goldhaber et al[45]
0.1	4	1	$c\bar{c}$ model, Lane et al[24,47]
0.2 ±0.1	4.5 ± 0.8	128 ±40	Goldhaber et al[45]
1	4	7	spin factors

TABLE III. Cross sections for D^o and D^+ production at different e^+e^- energies.[51] The last column gives the D contribution, $R_{D\bar{D}}$, to the total hadronic cross section expressed as a ratio to $\sigma_{\mu\mu}$.

E Interval (GeV)	$\langle E_{CM} \rangle$ (GeV)	σ_{D^o} (nb)	σ_{D^+} (nb)	$R_{D\bar{D}} = \frac{\sigma_{D^+} + \sigma_{D^o}}{2\sigma_{\mu\mu}}$
3.73 - 3.76	3.74	<1.7	<1.9	<0.29
3.76 - 3.79[a]	3.775	11.5 ±2.5	9.1 ±2.0	1.75 ±0.27
3.79 - 3.84	3.81	<0.7	<0.8	<0.13
3.84 - 3.89	3.87	2.1 ±1.4	1.1 ±1.1	0.28 ±0.16
4.028[b]	4.03	24.2 ±7.0	9.6 ±2.9	3.26 ±0.73
4.0 - 4.2	4.15	16.5 ±5.0	6.2 ±2.5	2.33 ±0.57
4.2 - 4.4	4.28	2.1 ±2.1	6.0 ±2.9	0.88 ±0.40
4.414[b]	4.41	12.6 ±4.2	7.8 ±3.0	2.36 ±0.60
4.4 - 5.0	4.68	9.5 ±3.7	8.9 ±3.1	2.30 ±0.60
5.0 - 5.8	5.36	5.6 ±4.4	2.0 ±2.0	1.30 ±0.83
6.0 - 7.8[c]	7.0	2.3 ±0.8	1.7 ±0.7	1.13 ±0.44

[a] The D cross sections at this energy, measured in Ref. 5, have been reported by I. Peruzzi et al.[53]

[b] These values are calculated by using the $\sigma \cdot B$ values measured by Piccolo et al[43] and the branching fraction B measured by Peruzzi et al.[53]

[c] From Rapidis et al.[52]

as decay products of D*. The values of $R_{D\bar{D}}$ are plotted in Fig. 15. The measurement of σ has been possible only recently, that is, after the LGW experiment has measured absolute branching ratios[53] for D decays at the ψ'' (as discussed in Section IV.D). In fact, when events are observed in a mass plot, as those of Fig. 8, the quantity measured is $\sigma \cdot B$, where B is the branching fraction for decay of the D into the final state being considered.

Of course, since D* mesons decay into D mesons, the inclusive D cross sections accounts also for the production of any excited states of the D. In addition to D mesons, F, F* and charmed baryons are expected to contribute to R_{charm} (see Section III.D).

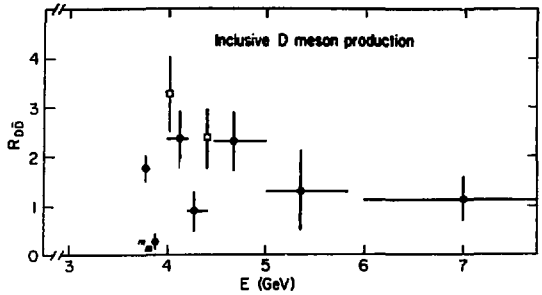

Fig. 15. The cross section for the reaction $e^+e^- \to D\bar{D}$ + anything expressed in units of $\sigma_{\mu\mu}$, $R_{D\bar{D}}$, as a function of energy.[51,52] The solid dots (●) represent the data of the LGW experiment,[51] the squares (▫) are calculated from the σ·B measurements of Piccolo et al.[43]

B. F Meson

The DASP collaboration has reported evidence for F production about a year ago.[54] They have observed five events of the type

$$e^+e^- \to F^+\overline{F^{*-}} \quad \text{(and c.c.)} \qquad \text{with} \qquad \begin{array}{l} F^\pm \to \eta\,\pi^\pm \\ \qquad\quad \hookrightarrow \gamma\,\gamma \\ F^{*\pm} \to F^\pm\,\gamma_{soft} \end{array} \tag{33}$$

at the 4.41 GeV resonance. They also observed that the cross section for η production at 4.41 GeV, $\sigma_\eta = 4.1 \pm 0.9$ nb, is much larger than elsewhere. This cross section corresponds to $R_\eta = 0.82$. The masses quoted are: $M_F = 2.03 \pm 0.06$ GeV and $M_{F^*} - M_F = 110 \pm 46$ MeV. As you have heard from Prof. Wolf in his lectures, the same DASP collaboration have now analyzed the data at 4.16 GeV and also observed a large η production cross section:[55] $\sigma_\eta = 1.8 \pm 1.2$ nb. The σ_η as a function of energy is shown in Fig. 16. It is consistent with zero at 4.03, 4.3 and 5.0 GeV, from which the authors infer that the peak at 4.16 GeV is an $F\bar{F}$ state and the 4.41 peak is an $F\bar{F}^*$ state, with the η production showing the same trend. They also find that the fraction of $F \to \eta\pi$ is:

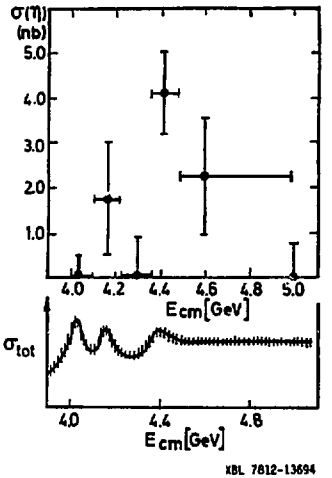

Fig. 16. Inclusive η cross section in e^+e^- annihilation as measured by the DASP experiment.[55] The bottom curve shows the trend of total hadronic cross section as measured by DASP.[18] Plot taken from Flügge.[20]

$$\frac{B(F \to \eta\pi)}{B(F \to \eta + \text{anything})} = 0.09 \pm 0.04 \qquad (34)$$

therefore at 4.16 GeV they find

$$\sigma(e^+e^- \to F\bar{F}) \cdot B(F \to \eta\pi) = 0.08 \pm 0.06 \text{ nb} \qquad (35)$$

where the error is so large because of large uncertainties in the η detection efficiency, which depends not only on the acceptance of the apparatus, but also on the details of the assumed production mechanism.

The lead-glass wall experiment has reported some indication of F production in the $K\bar{K}\pi$ channel.[56] We have reanalyzed that data and will now present the results.

We have studied all channels with a $K\bar{K}$ pair, which should be the other copious decay mode expected for the F. The following final states have been analyzed at 4.16 GeV (the sample had a total integrated luminosity of 940 nb^{-1}):

$$e^+e^- \rightarrow K^+K^-\pi^\pm + X \qquad (36a)$$

$$K^+K^-\pi^+\pi^-\pi^\pm + X \qquad (36b)$$

$$\rightarrow K^+\bar{K}^o + X \qquad \text{(and c.c.)} \qquad (36c)$$

$$K^+\bar{K}^o\pi^+\pi^- + X \qquad \text{(and c.c.)} \qquad (36d)$$

$$K^o\bar{K}^o\pi^\pm + X \qquad (36e)$$

where X stands for anything else, either charged or neutral particles.

The K^o's were identified by measuring the dipion mass as mentioned in Section III.A.1 and the charged K by time of flight. Since for each track we measure the time of flight, the path length and the momentum we can calculate the confidence level (CL) for it to be a π, K or proton. A particle is chosen to be a K if $(CL)_\pi < (CL)_K > (CL)_p$. This method is reliable up to momenta of 0.9 GeV ($\sigma_{TOF} = 0.4$ ns), which is the range of momenta relevant for reactions (36).

The mass resolution was also improved by using the same method applied for the precise mass measurements of the D meson,[53] which will be described in Section IV.A.1. It consists of selecting those events in which the total energy of the $K\bar{K}(n\pi)$ system is within 60 MeV of the beam energy and then replacing the measured total energy of these particles with the beam energy (whose energy resolution is 1 MeV). For these events the likely reaction is a two-body process with equal mass for the two bodies, as expected, if the reaction $e^+e^- \rightarrow F\bar{F}$ were to take place.

A total of 86 events were found with these criteria for the above reactions with $M(K\bar{K}\ n\pi) > 2.0$ GeV. The invariant mass distribution of the $K\bar{K}(n\pi)$ combinations for these events is shown in Fig. 17. The only significant deviation from a flat distribution is found at M = 2040 MeV. Notice that the events are plotted in 2 MeV bins and that the signal is practically all in two bins. This agrees with the expected resolution at this mass. The significance of this signal is not very high. There are 14 events where 4.2 would be expected; this corresponds to a probability of 1.3×10^{-4} for a Poisson distribution. In terms of standard deviations, the significance of the effect is at the 4 standard deviation level. Therefore, we are not prepared to say that we have an F signal. However, since the mass at which we observe this effect is in the general mass region where the DASP collaboration reported an F signal, we can make some comparisons.

Assuming that this 4 standard deviation effect is due to F

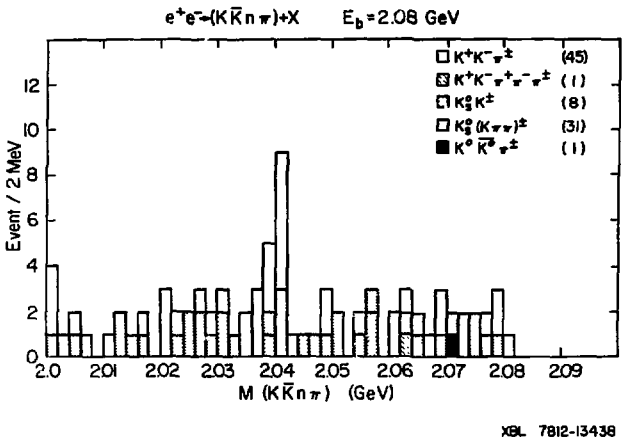

Fig. 17. Invariant mass distribution of the ($K\bar{K}n\pi$) system as obtained by the LGW experiment. Five different channels contribute, their symbols and number of events are shown in the plot. See text for more details.

production, from the $K^+K^-\pi^\pm$ channel we get

$$\sigma(e^+e^- \to F\bar{F}) \cdot B(F^+ \to K^+K^-\pi^+) = 0.10 \pm 0.05 \text{ nb} \qquad (37)$$

where the error includes the contribution from the uncertainty in the detection efficiency for this final state.

Comparing Eqs. (35) and (37) we observe that if the signal in Fig. 17 were due to the F meson

$$r = \frac{B(F^+ \to K^+K^-\pi^+)}{B(F^+ \to \eta\pi^+)} = 1.2 \pm 1.1 \qquad (38)$$

in agreement with theoretical expectations. In fact, the predictions of the statistical model of Quigg and Rosner[57] is r = 1.1 and the QCD calculations of Cabibbo and Maiani,[58] (to be discussed in more detail in Section IV.D.3 for D decays) give r = 0.96.

One further speculation involves the comparison of the overall $K\bar{K}(n\pi)$ rate with the overall $\eta(n\pi)$ rate. This comparison can be done by using the statistical model to calculate the acceptance. The average acceptance for the channels listed in Eqs. (36) is $\varepsilon = 0.027$ with a large uncertainty. The total cross section then is

$$\sigma(e^+e^- \to F\bar{F}) \cdot B(F \to K\bar{K}(n\pi) \text{ of Eqs. (36)}) = 0.23 \pm 0.10 \text{ nb} . \quad (39)$$

According to the statistical model[57] the detected channels constitute 60% of all the $K\bar{K}(n\pi)$ channels. Using this factor we can compare (39) with the total η cross section assuming that it all comes from $F \to \eta(n\pi)$. Of course, since the semileptonic decays are also included, this means overestimating the $F \to \eta(n\pi)$ cross section. We get

$$\frac{B(F \to \eta(n\pi))}{B(F \to K\bar{K}(n\pi))} = 4 \pm 3$$

The statistical model predicts a value of about two for this ratio.

C. Charmed Baryons

There has been no observation of a peak in an invariant mass distribution which could be interpreted as charmed baryon production in e^+e^- collisions.

Cazzoli et al[59] first reported a candidate for a charmed baryon in a neutrino experiment in the BNL hydrogen bubble chamber. They found one event of the type

$$\nu p \to \mu^- \Lambda \pi^+ \pi^+ \pi^+ \pi^- \quad .$$

This reaction violates the $\Delta S = \Delta Q$ rule in weak interactions, but it would be allowed if a charmed baryon ($\Lambda_c^+ \to \Lambda\pi^+\pi^+\pi^-$) were being produced. The mass of the Λ_c^+ using this event was measured to be 2.26 GeV. Subsequently a Fermilab photoproduction experiment[60] observed a peak at the same mass in the $\bar{\Lambda}\pi^-\pi^-\pi^+$ mass spectrum.

The *only* indication of charmed baryon production in e^+e^- collisions comes from the inclusive baryon cross section measured at SPEAR. The data,[61] a combination of the SP17 and SP26 experiments, are shown in Fig. 18. We have measured the inclusive $\bar{p}$, Λ and $\bar{\Lambda}$ cross sections in the energy region 3.82 to 7.36 GeV. The antiprotons were identified by time-of-flight and momentum measurements, the Λ and $\bar{\Lambda}$ by study of the invariant mass of the $p\pi^-$ and $\bar{p}\pi^+$ combinations, which show peaks at the appropriate mass. Figure 18a shows the ratio $R = \sigma/\sigma_{\mu\mu}$ for production of p and $\bar{p}$.

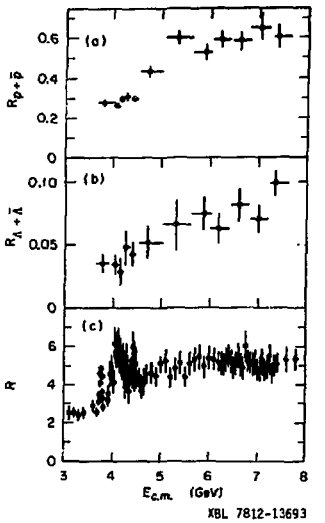

Fig. 18. Inclusive measurement[61] of $R(p+\bar{p})$ shown in graph (a), and $R(\Lambda+\bar{\Lambda})$ shown in graph(b). The measurement of R, the total hadronic production, is shown for comparison in (c) (see Fig. 2 for references).

This is actually $R(p+\bar{p}) = 2R_{\bar{p}}$, since the proton cross section is more difficult to measure because of the large background due to beam-gas interactions. Figure 18b shows the same ratio for $\Lambda+\bar{\Lambda}$ production.

The values of $R(p+\bar{p})$ exhibit a sharp rise of $\Delta R = 0.3$ between 4.4 and 5 GeV. Using the mass for Λ_c mentioned above and the mass formula of De Rujula et al,[62] the thresholds for associated production of charmed baryon pairs ($\Lambda_c^+\bar{\Lambda}_c^-$, $\Sigma_c\bar{\Sigma}_c$, $\Sigma_c^*\bar{\Sigma}_c^*$) are expected to be in this energy region. $R(\Lambda+\bar{\Lambda})$ also shows an increase in the same energy region, although the statistics are not as good and the rise is not as sharp. However, from Fig. 18b we can estimate that the maximum value of $\Delta R(\Lambda+\bar{\Lambda})$ could be ~0.04 or about 10-15% of $\Delta R(p+\bar{p})$. This observation indicates that charmed baryon decays into Λ, Σ^0, and therefore $\Sigma^\pm$ are smaller than decays into strange mesons and nucleons (like $\bar{K}^0p$ or $K^-p\pi^+$).

Prior to the LGW experiment a UCLA group had modified the Mark I magnetic detector in order to identify the $\bar{n}$ and $\bar{p}$ produced. They have measured, as reported by Ferguson et al.,[83] the $\bar{\Sigma}^\pm$ production at 4 and at 7 GeV total energy. They find an increase between these two energies of $\Delta R(\bar{\Sigma}^\pm) = 0.12 \pm 0.05$, somewhat larger than the $\bar{\Lambda}$ result. Although the errors are large, these two results seem to be in disagreement.

D. Summary of Contributions to R

We can now summarize what we have learned so far on the total hadronic cross section, that is, on various contributions to $R = \sigma_h/\sigma_{\mu\mu}$. We have to point out at this point that, since the detectors that have measured R do not cover 100% of the solid angle, all the R measurements depend strongly on Monte Carlo calculations to correct for the events that have not triggered the apparatus. The systematic errors associated with these calculations are estimated to be ±15% for the SPEAR magnetic detector,[4] ±20% for the DELCO detector,[48] ±15% for DASP,[18] and ±11% for PLUTO.[50] The general features in R are similar (see Figs. 2, 13 and 14) but there are differences in the details as already mentioned in discussing the effects in the 3.95 and 4.16 GeV energy regions (see Section III.A.2). The R measured by PLUTO[50] is systematically lower than those measured by other detectors. Because of these problems we will discuss the different contributions to R within the same detector, that is, the SLAC-LBL Mark I detector, since both $R_{D\bar{D}}$ and the contribution from charmed baryons were measured in this detector.

The values of R as measured in the Mark I detector[4,5] are shown in Fig. 2. Since there is a high density of data points in this figure, we have drawn by hand a curve to represent these data so that we can compare it with the sum of the different parts that we have measured and discussed in the previous sections. This curve is shown in Fig. 19. As for the individual contributions to R we can say the following:

1. These data indicate R = 2.5 below charm threshold, so we will assume that this is the contribution of the old quarks u, d, and s.
2. The heavy lepton contribution to R can be calculated from QED to be $R_{\tau^+\tau^-} = \beta(3-\beta^2)/2$.
3. The charmed baryon contribution $R_{B\bar{B}}$ has been added in with a value that rises from 0 to $\frac{1}{2}(0.64) = 0.32$ between 4.4 and 5 GeV (the $n+\bar{n}$ contribution is assumed to be the same as that of $p+\bar{p}$). Above 5 GeV it is assumed to be constant as indicated by the data of Fig. 18a.
4. Finally, the $R_{D\bar{D}}$ values of Fig. 15 and Table III have been added to the above as points with error bars.

The sum of these contributions appears to saturate the measured values of R. However, the uncertainties of the $R_{B\bar{B}}$ and $R_{D\bar{D}}$ measurements are such that ½ unit of R of F production or some other process could be easily accommodated.

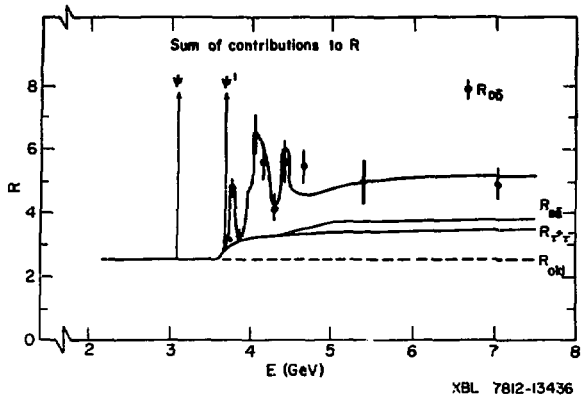

Fig. 19. A composite graph illustrating the various contributions to R, the total hadronic cross section over $\sigma_{\mu\mu}$. The top curve is a sketch of R, hand drawn over the data of Fig. 2. The following contributions are progressively added starting from R = 0: R_{old} is a constant as inferred by the data points below charm threshold; $R_{\tau^+\tau^-}$ is the heavy lepton contribution as calculated from QED; $R_{B\bar{B}}$ is the charmed baryon contribution as inferred by the data[61] of Fig. 18. Finally we add the contribution[51,52] of $R_{D\bar{D}}$ as data points, taken from Fig. 15 and Table III.

IV. PROPERTIES OF CHARMED MESONS

In this section we will review masses and branching ratios for D and D*. In addition, we will review the situation on D^0 and $\bar{D}^0$ mixing. Due to the time available for these lectures, we will not review the spin and parity assignments of the D mesons. Detailed studies made by the SLAC-LBL collaboration[63] find that indeed the D has $J^P = 0^-$.

A. Masses of D and D* Mesons

The mass of a particle found as a peak in an invariant mass of n particles can be calculated with the expression

$$M = \sqrt{\left(\sum_i E_i\right)^2 - \left(\sum_i \vec{p}_i\right)^2} \qquad (40)$$

where the sums are over the n particles.

1. D Masses. As already mentioned, the LGW experiment was able to measure[53] the D masses with high precision at the $\psi(3772)$ for the following reasons:

   a. The D production is the two-body process $e^+e^- \to D\bar{D}$ because there is not enough energy for any additional particles. For this process the D energy is equal to the beam energy and we can substitute E_b for $\sum_{i=1}^{n} E_i$ in Eq. (40). This fact improves the resolution considerably because the r.m.s. error[64] of E_b is 1 MeV. Thus E_b is much better determined than the energy obtained by the momentum measurement of the n tracks.

   b. The momenta of the secondary particles are low, $p_D \sim 300$ MeV/c. Therefore, the uncertainty on p_D contributes very little to the uncertainty on the mass of the D.

The overall resolution is 3 MeV and the final error on the D mass is dominated by the systematic errors rather than the statistical error.

The invariant mass distributions for the various observed decay channels of the D^+ and D^0 are shown in Fig. 20. Here the charged and neutral kaons have been identified with the same methods described earlier (see Section III.A.1). Among all the hadronic events at the ψ'' peak of Fig. 10, we have chosen those for which $\sum_i E_i$, that is, the measured E_D, is within 50 MeV of the beam energy. For these combinations of n particles

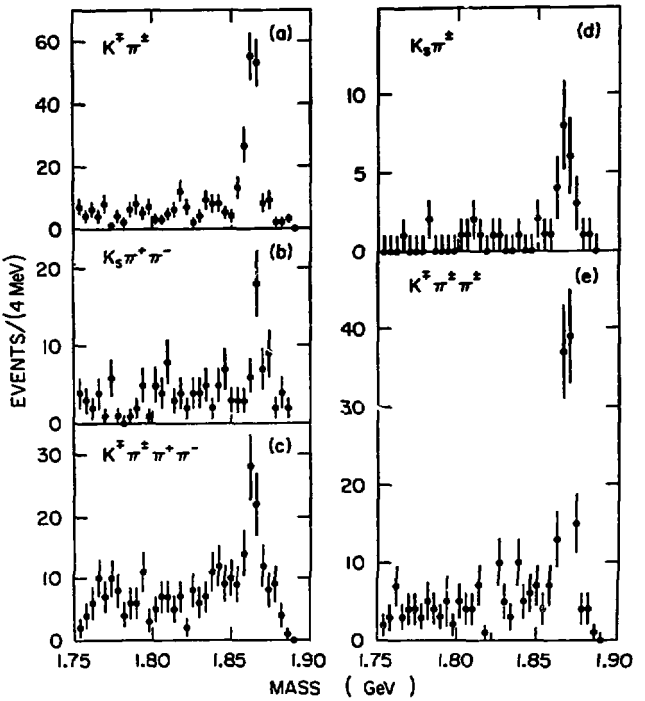

Fig. 20. Invariant mass spectra for various D^o (on the left) and D^+ (on the right) decay modes. Note that the distributions are plotted in 4 MeV bins.

we use Eq. (40) to calculate the invariant mass with E_b instead of $\sum_i E_i$. Fits to the combined distributions for D^o and D^+ give the mass values

$$M_o = 1863.3 \pm 0.9 \text{ MeV} \quad (41)$$

$$M_+ = 1868.3 \pm 0.9 \text{ MeV} \; . \quad (42)$$

The major systematic uncertainties contributing to the errors are: 0.5 MeV from the long-term stability of the E_b monitoring and 0.5 MeV from the absolute momentum calibration. The error on the $D^+ - D^o$ mass difference, shown in Table IV, is smaller than either of the *D* mass errors because some of the systematic errors cancel out.

TABLE IV. Masses, mass differences, and Q values for the D meson system.[53] The quantities in parentheses are taken from Refs. 45 and 65 and are used in the calculation of quantities involving D*'s. All units are in MeV. See text for a discussion of the errors.

Mass (MeV)		Mass Difference (MeV)		Q Values (MeV)	
D^o	1863.3±0.9	$D^+ - D^o$	5.0±0.8	$D^{*o} \to D^o\pi^o$	7.7±1.7
D^+	1868.3±0.9	$D^{*+} - D^{*o}$	2.6±1.8	$D^{*o} \to D^+\pi^-$	-1.9±1.7
D^{*o}	(2006.0±1.5)	$(D^+-D^o)-(D^{*+}-D^{*o})$	2.4±2.4	$D^{*+} \to D^o\pi^+$	(5.7±0.5)
D^{*+}	2008.6±1.0	--	--	$D^{*+} \to D^+\pi^o$	5.3±0.9

2. D* Masses. Measurements relevant to the D* masses come from the SP17 experiment. The best measured quantities are the D^{*o} mass[45] and the Q value[65] of the decay $D^{*+} \to D^o\pi^+$, which are shown in Table IV.

For the D^{*o} they used essentially the same method described for the D. That is, at 4.03 GeV they used the reaction $e^+e^- \to \bar{D}^{*o}D^{*o}$ with $D^{*o} \to D^o\pi^o$. For this two-body reaction the energy of the D^{*o} is, of course, E_b. As for the momentum of the D^{*o}, they assume it to be equal to the measured D^o momentum with a little correction due to the unmeasured π^o. Again the Q of the reaction is small, the momentum of the D^{*o} is small, and its error contributes little to the error on the D^{*o} mass. From Eq. (40) M can be calculated.

The P_D distribution is shown in Fig. 21. The detailed fit[45] of this distribution will be described in Section IV.C. For the

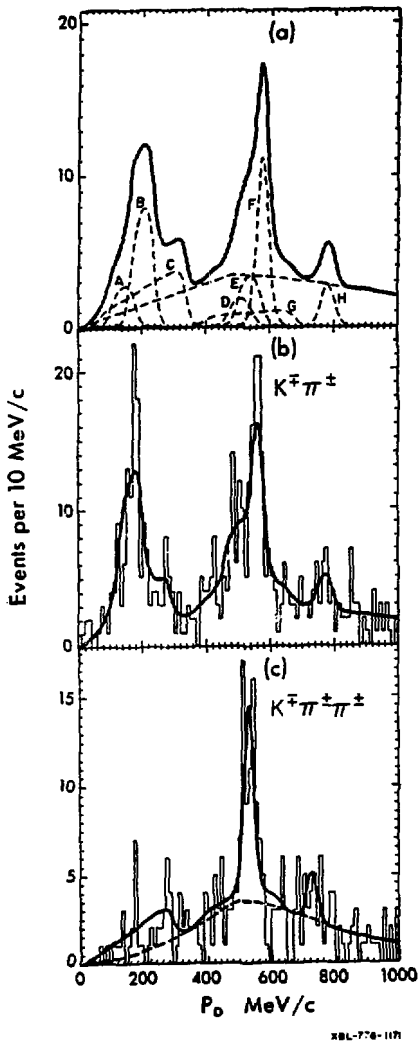

Fig. 21. Studies of p_D at 4.03 GeV.[45] (a) Contribution to the expected D^o momentum spectrum from

A $e^+e^- \rightarrow D^{*+}D^{*-}$, $D^{*+} \rightarrow \pi^+D^o$

B $\rightarrow D^{*o}\bar{D}^{*o}$, $D^{*o} \rightarrow \pi^oD^o$

C $\rightarrow D^{*o}\bar{D}^{*o}$, $D^{*o} \rightarrow \gamma D^o$

D $\rightarrow D^{*+}D^-$, $D^{*+} \rightarrow \pi^+D^o$

E $\rightarrow D^{*o}\bar{D}^o$, $D^{*o} \rightarrow \pi^oD^o$

F $\rightarrow \bar{D}^{*o}D^o$, direct D^o

G $\rightarrow D^{*o}\bar{D}^o$, $D^{*o} \rightarrow \gamma D^o$

H $\rightarrow D^o\bar{D}^o$ direct D^o

(b) $D^o \rightarrow K^-\pi^+$ momentum spectrum, the curve is the result of the fit and (c) $D^+ \rightarrow K^-\pi^+\pi^+$ momentum spectrum where the curve is the result of the fit and the dashed line is the background.

D^{*o} mass the main uncertainty comes from the determination of the center of the peak B (see Fig. 21a) due to $D^{*o} \to D^o\pi^o$ in the presence of peak A due to $D^{*+} \to D^o\pi^+$ and peak C due to $D^{*o} \to D^o\gamma$. The fit gives the value

$$M_{D^{*o}} = 2006.0 \pm 1.5 \text{ MeV} \qquad (43)$$

The same method has been used for the D^{*+} mass measurement,[45] but due to smaller statistics (Fig. 21c), the errors are twice as large. The best information on the D^{*+} mass comes from direct observation[65] of $D^{*+} \to D^o\pi^+$ at 6.8 GeV where the π^+ momentum is large enough to be measured in the magnetic detector. Again, the Q of the reaction $D^{*+} \to D^o\pi^+$ is small and can be determined accurately. Figure 22a shows the $D^{*+} - D^o$ mass difference which

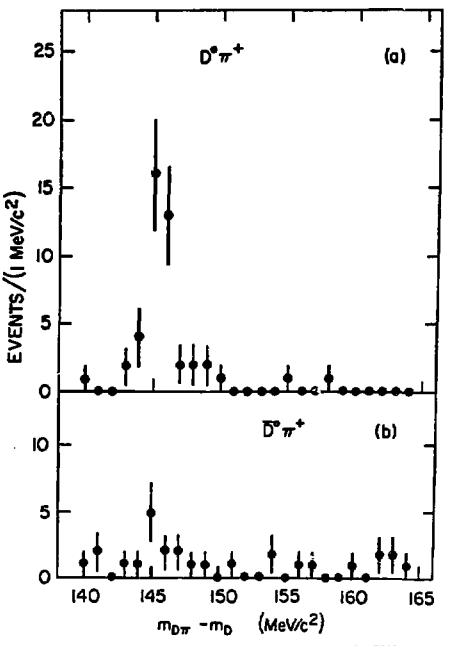

Fig. 22. Study[65] of $D^{*+} \to D^o\pi^+$; the $D\pi$-D mass difference is shown (a) for $D^{*+} \to D^o\pi^+$ with $D^o \to K^-\pi^+$, and (b) for the sequence $D^{*+} \to \bar{D}^o\pi^+$ with $\bar{D}^o \to K^+\pi^-$. Events from the charge conjugate reactions are included.

gives

$$Q(D^{*+} \to D^{o}\pi^{+}) = 5.7 \pm 0.5 \text{ MeV} \qquad (44)$$

This value is shown in Table IV and in combination with the D^{o} mass, gives the D^{*+} mass shown in the table.

The remaining values in Table IV, essentially the $D^{*+} - D^{*o}$ mass difference and the Q values for D* decays, are quantities derived from the directly measured ones. The quoted errors take into account that some of the systematic errors cancel out in the difference. The Q values for the D* decays are shown in Fig. 23.

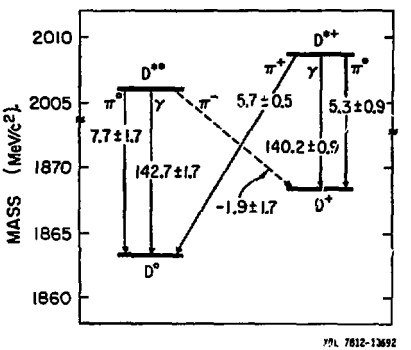

Fig. 23. Mass level diagram for D* and D^{o} states from the measurements shown in Table IV. The arrows represent different decay modes of the D*; the numbers across the lines represent the Q for each decay expressed in MeV. The decay $D^{*o} \to D^{+}\pi^{-}$ cannot take place.

The decay $D^{*o} \to D^{+}\pi^{-}$ is not energetically possible. This observation was already reported before the precise mass measurements of Ref. 53.

3. Charged-Neutral D and D* Mass Differences. Expectation for the masses of charmed particles have been discussed by De Rujula, Georgi, and Glashow[62] (see also Jackson's review[1]). We only mention here the prediction for the mass splitting of members of the same isotopic spin multiplet. The experimental results in

Table IV show that

$$\delta = M_{D^+} - M_{D^0} = 5.0 \pm 0.8 \text{ MeV} \quad (45)$$

$$\delta^* = M_{D^{*+}} - M_{D^{*0}} = 2.6 \pm 1.8 \text{ MeV} . \quad (46)$$

For comparison

$$M_{K^+} - M_{K^0} = -4.01 \pm 0.13 . \quad (47)$$

In the non-relativistic quark model the mass splittings are

$$\delta = M_{D^+} - M_{D^0} = (m_d - m_u) + \frac{2}{3}\alpha\left[\left\langle\frac{1}{r_D}\right\rangle + \frac{2\pi}{m_c m_u}|\psi_D(o)|^2\right] \quad (48)$$

$$\delta^* = M_{D^{*+}} - M_{D^{*0}} = (m_d - m_u) + \frac{2}{3}\alpha\left[\left\langle\frac{1}{r_D}\right\rangle - \frac{2\pi}{3m_c m_u}|\psi_D(o)|^2\right] \quad (49)$$

where the first term is the d-u quarks mass difference, the second term is a contribution from single photon exchange. Using current algebra for $m_d - m_u$ and an atomic quark model similar to charmonium for the second term, Lane and Weinberg[67] find $M_{D^+} - M_{D^0} = 7$ MeV to be compared with Eq. (45) and $M_{D^{*+}} - M_{D^{*0}} = 6.5$ MeV. The calculation by De Rujula et al[66] gave 15 MeV for the D mass difference (45). Finally we find

$$\delta - \delta^* = 2.4 \pm 2.4 \text{ MeV} . \quad (50)$$

This is an electromagnetic hyperfine splitting and is expected to be ~1 MeV in most theoretical models.

B. $D^0 - \bar{D}^0$ Mixing

Mixing of the D^0 and $\bar{D}^0$ states could arise from $\Delta C = \Delta S$ and $\Delta C = -\Delta S$ transitions of the c quark, as in the two diagrams below

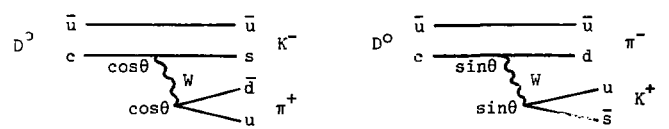

It turns out, however, that the mixing due to these diagrams is smaller than expected from the $\tan^2\theta$ ratio of the amplitudes[36] and is negligible. One other possible source of D^0-$\bar{D}^0$ mixing is the

charm changing neutral current,[69] if it were to exist. In this case one would expect D^0-$\bar{D}^0$ mixing to be complete. Therefore it is very important to check out this hypothesis experimentally.

The only experimental data on D^0-$\bar{D}^0$ mixing was obtained from the SLAC-LBL experiment SP17 in two separate studies. The first[65] was done with D^{*+} produced in the 5 to 7.8 GeV energy region. The reaction studied was

$$e^+e^- \rightarrow D^{*+} + X \qquad \text{(and c.c.)} \tag{51}$$

with

$$D^{*+} \rightarrow D^0\pi^+ \quad \text{and} \quad D^0 \rightarrow K^-\pi^+ \tag{52a}$$

or

$$D^{*+} \rightarrow \bar{D}^0\pi^+ \quad \text{and} \quad \bar{D}^0 \rightarrow K^+\pi^- \tag{52b}$$

and their charge conjugates. Here for D^0-$\bar{D}^0$ mixing, one would expect to detect some events with $D^{*+} \rightarrow \bar{D}^0$. The data is shown in Fig. 22b. Five events are observed in the correct mass region compared with the 26 events above background in Fig. 22a. After corrections, these events give an upper limit

$$\frac{N(\text{wrong sign K})}{\text{all } D^{*+} \text{ events}} < 16\% \text{ with } 90\% \text{ CL} .$$

The second study[45] was made on the reaction

$$e^+e^- \rightarrow D^0 + K^\pm + X ,$$

that is, the sign of the K accompanying the D^0 is the signal for D^0-$\bar{D}^0$ mixing. For no D^0-$\bar{D}^0$ mixing one expects strangeness conservation, that is, a K^+ should accompany a D^0. The result of this study is

$$\frac{N(\text{wrong sign K})}{\text{all } D^0 \text{ events}} < 18\% \text{ with } 90\% \text{ CL} .$$

The above results exclude complete $D^0 - \bar{D}^0$ mixing.

C. D* Branching Fractions

The measurements of the D* branching fractions have been made by Goldhaber et al[45] at the 4.03 GeV bump in the cross section. As already discussed in Section III.A.2, at this energy there is a large $D^*\bar{D}^*$ production. The measurements are done through the study of the momentum of the D meson detected: the momentum is different depending upon the D* decay mode it comes from, as well as upon the D* or D production reaction. This is illustrated in

Fig. 21a. The curves A through H represent the various possible ways to obtain a D^0 either from decays of D^* or directly. Figure 21 shows the result of a simultaneous fit to the D^0 and D^+ data. These curves were obtained with the following assumptions:

a. The production of D^0 or D^+ processes are the ones shown in Fig. 21a, with the addition of direct D^+D^- production.

b. The decay modes for D^{*0} and D^{*+} are the ones shown in Table V. In fact, $D^{*0} \to D^+\pi^-$ is not energetically possible (see Fig. 23), so the fractions of $D^{*0} \to D^0\pi^0$ and $D^{*0} \to D^0\gamma$ should add to unity.

c. Only three ratios,

$$B(D^{*0} \to \gamma D^0) \tag{53}$$

$$B(D^{*+} \to \pi^+ D^0) \tag{54}$$

and

$$\frac{B(D^+ \to K^-\pi^+\pi^+)}{B(D^0 \to K^-\pi^+)} \tag{55}$$

were left free to vary. In order to fit these parameters an isospin-constrained fit was done, so that $D^{*+} \to \pi^+D^0$ and $D^{*+} \to \pi^0D^+$ are related by isospin coefficients.

d. The ratio $\Gamma(D^{*+} \to \gamma D^+)$ over $\Gamma(D^{*0} \to \gamma D^0)$ was assumed from theory[70] to be 1/4. For much smaller values the data with $p_{D^0} \leq 300$ MeV/c could not be fitted easily.

The results for the D* branching fractions are shown in Table V. For a discussion about how sensitive these results are to the assumptions made, the reader is referred to Ref. 45. The quoted errors, however, take into account the uncertainties related to the model dependence of the fit.

Table V also gives the most recent theoretical predictions for these decays, as estimated by Eichten et al.[47] For the $D^* \to D\gamma$ they use the naive quark model formula

$$\Gamma(D^* \to D\gamma) = \frac{4}{3}\alpha\left(\frac{Q_c}{2m_c} + \frac{Q_i}{2m_i}\right)^2 p^3 \tag{56}$$

where $Q_c = 2/3$ and Q_i are the quark charges involved ($Q_u = 2/3$ for D^0 and $Q_d = 1/3$ for D^+); $m_c = 1.87$ GeV, as determined in their linear potential calculation using $\Gamma(\psi \to e^+e^-)$ and $M_{\psi'}-M_\psi$ as input

TABLE V. D* branching fractions as measured by Goldhaber et al[45] compared with theoretical expectation.[47]

Mode	Experiment[45] (in %)	Theory[47] (in %)
$D^{*o} \to D^o\pi^o$	$(45 \pm 15)^a$	53.0
$\to D^o\gamma$	55 ± 15^a	47.0
$D^{*+} \to D^+\pi^o$	$(30 \pm 7)^b$	28.4
$D^o\pi^+$	60 ± 15	68.4
$D^+\gamma$	$(10 \pm 17)^c$	3.2

[a] The free parameter in the fit was $D^* \to D^o\gamma$, the sum of the two decays was constrained to one.

[b] Value derived from $D^{*+} \to D^o\pi^+$ using isospin factors.

[c] Obtained as difference from unit once the $D^* \to D^o\pi^+$ is determined.

data; $m_u = m_d = 0.33$ GeV; finally $p = (1/2M_{D^*})(M_{D^*}^2 - M_D^2)$.

The $D^* \to D\pi$ width was obtained by assuming a form derived from their $q\bar{q}$ model for higher ψ levels decaying into $D\bar{D}$:

$$\Gamma(D^* \to D\pi) = \frac{p^3}{72\pi M_{D^*}^2} C^2 \left| \sqrt{M_{D^*} E_D E_\pi}\, A \right|^2 \qquad (57)$$

where E_i is the D or π energy, p their momentum, C a Clebsch-Gordan coefficient, and A is an amplitude depending only on m_u (for $m_c \to \infty$). A can be estimated from $K^* \to K\pi$ under the assumption that m_s is very large. This gives

$$A = 47.8 \text{ GeV}^{-3/2} .$$

The estimated branching fractions with these assumptions are shown in Table V. They are in good agreement with the experimental results.

D. Decay Properties of the D Meson

Some hadronic branching fractions of the D have been measured at the $\psi(3772)$ by the LGW experiment.[53] The semileptonic branching fraction has been measured both at SPEAR and at DORIS. The LGW experiment has also measured some inclusive characteristics of the D decays,[71] again at the $\psi(3772)$. A review on all that is known today on D decays follows.

1. Hadronic Decay Modes. As mentioned in Section III.A.1, the SPEAR magnetic detector experiment SP17 has detected a number of D decays[41-43] (see Fig. 8). However, absolute branching fractions were not measured until later, that is, until the D's were copiously produced at the $\psi(3772)$, where it has been possible to measure the cross section for D production.

As discussed in Section III.A.2, one can assume that the ψ'' decays entirely into $D\bar{D}$, therefore the cross section for $D\bar{D}$ production is equal to the resonant cross section,[5] shown in Fig. 10. As for the ratio of D^o to D^+ production, reactions (30) and (31), it is reasonable to assume[53] that it is given by the ratio of the kinematical and barrier factors present in the p-wave Breit-Wigner formula. These cross sections are shown in Table III.

Figure 20 shows the invariant mass distribution for a number of $K(n\pi)$ mass combinations. These distributions were obtained as explained in Section IV.A.1. If N_i is the number of events found in channel i, we write

$$N_i = 2\sigma(e^+e^- \to D\bar{D})\, B_i\, A_i\, L \qquad (58)$$

where B_i and A_i are the branching fraction and the acceptance of the apparatus for D decaying into that channel, L is the integrated luminosity of the sample analyzed, and the factor 2 is present because either D can decay into that channel. The branching fractions calculated in this way are shown in Table VI. Here the decay $D^o \to K^-\pi^+\pi^o$, also observed at the $\psi(3772)$ by the LGW experiment,[72] has been added as well as the semileptonic decay fraction measured[73] in the same experiment. For more details on the methods used to measure these branching ratios as well as for a review of LGW results, see Ref. 74.

In Table VI we notice the following:

a. The $D^+ \to \bar{K}^o\pi^+$ decay mode is observed. Comparison with the $D^o \to K^-\pi^+$ decay mode gives

$$\frac{\Gamma(D^+ \to \bar{K}^o\pi^+)}{\Gamma(D^o \to K^-\pi^+)} = (0.70 \pm 0.23)\,\frac{\tau_o}{\tau_+} \qquad (59)$$

where τ_o and τ_+ are the lifetimes of the D^o and the D^+. The value (59) shows that if the two lifetimes are not too different, the $D^+ \to \bar{K}^o\pi^+$ decay is of the same order of magnitude as the $D^o \to K^-\pi^+$ decay mode as predicted by Ellis et al[38] (see Section II.C.3). This result is relevant to the understanding of the nonleptonic enhancement and will be discussed in Section IV.D.3 below.

b. We have measured so far only a small fraction of the D decay modes into hadrons:

$$\sum_{\substack{\text{measured}\\ \text{modes}}} B_i(D^o \to \text{hadrons}) = (21.4 \pm 6.3)\% \qquad (60)$$

$$\sum_{\substack{\text{measured}\\ \text{modes}}} B_i(D^+ \to \text{hadrons}) = (5.4 \pm 1.2)\% \qquad (61)$$

Clearly more data is needed to fully understand the D decay properties.

Table VI shows that the three and four body final states are more copious than the two body final states. It is interesting to find out if there is resonance production in the D decays, that is, if there is evidence for reactions of the type

$$D \to K^*\pi, \quad K\rho, \quad K^*\rho, \quad \text{etc.} \qquad (62)$$

This question has been addressed by Piccolo et al.[43] They find the following:

a. No evidence[75] for K* production in the reaction
$$D^+ \to K^-\pi^+\pi^+$$

b. No evidence[43] for K* production or ρ production in the reaction
$$D^o \to \bar{K}^o\pi^+\pi^-$$

c. Evidence for ρ production in the reaction
$$D^o \to K^-\pi^+\pi^+\pi^-$$

For the last decay they find

Phase Space	$K^-\pi^+\rho^o$	$K^*\pi^+\pi^-$	$K^*\rho^o$
$0.05^{+0.11}_{-0.05}$	$0.85^{+0.11}_{-0.22}$	$0.0^{+0.2}_{-0.0}$	$0.10^{+0.11}_{-0.10}$

TABLE VI. Summary of D decay modes and branching fractions measured by the LGW experiment.[53,72,73]

Mode	B (%)
$D^0 \to K^-\pi^+$	2.2 ± 0.6
$\bar{K}^0\pi^+\pi^-$	4.0 ± 1.3
$K^-\pi^+\pi^-\pi^+$	3.2 ± 1.1
$K^-\pi^+\pi^0$	12 ± 6
$\bar{K}^0\pi^+\pi^-\pi^+\pi^-$	seen
e^+X [a]	7.2 ± 2.6
$D^+ \to \bar{K}^0\pi^+$	1.5 ± 0.6
$K^-\pi^+\pi^+$	3.9 ± 1.0
$\bar{K}^0\pi^+\pi^-\pi^+$	seen
e^+X [a]	7.2 ± 2.6

[a] The quantity measured is an average value for the D^+ and D^0 mesons. Here we assume that the two branching fractions are the same. See Section IV.D.2 for more details.

2. Semileptonic Decays. Evidence for anomalous electron production as a signature for D production and decay into an electron was first reported by the DASP group[76] in events with more than three charged prongs, that is, two charged prongs in addition to the electrons. The semileptonic branching fractions measured by different experiments are summarized in Table VII. Before we discuss the results we point out some characteristics of the events containing decays of D mesons and some difficulties in measuring the branching fractions.

a. The charmed particle decays with an electron are less affected by background in the multiprong events ($n_{ch} \geq 3$). The other source of anomalous electron production at these energies is the τ lepton.[30] The τ is expected to decay about 75% of the time into one charged prong. Therefore it is produced most copiously in 2-prong events, whereas the multiprong events ($n_{ch} \geq 3$) have a smaller contribution from this source. We will see that for events with $n_{ch} \geq 3$, one of which is an electron, the τ background is expected to be ~25% (see for example Fig. 24).

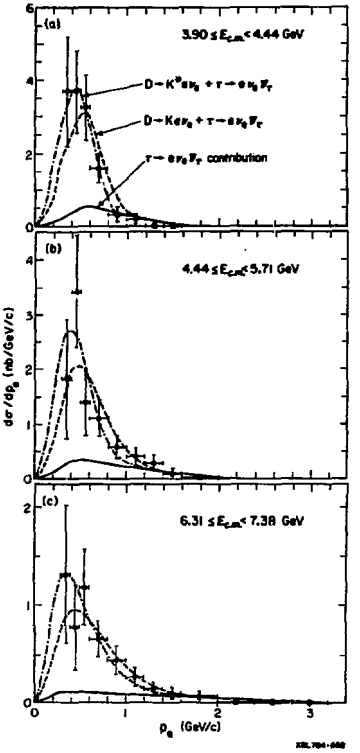

Fig. 24. The momentum spectrum for electrons produced in events with $n_{ch} \geq 3$ in three different energy intervals as obtained by the LGW experiment.[77] The curves are labeled in (a) and the energy intervals are indicated in each graph.

TABLE VII. The branching fraction for D semileptonic decay into electrons as measured by various experiments. For E > 4.08 GeV other charmed particles may contribute to the measurement.

E (GeV)	Electron events	Background events	Branching fraction (%)	Reference
3.772	61	25	7.2 ±2.8	LGW[73]
3.90 - 7.38	448	155	8.2 ±1.9	LGW[77]
3.99 - 4.08	-[a]	-[a]	8.0 ±2.0	DASP[78]
3.99 - 5.20	182	27	7.2 ±2.0	DASP[78]
3.77	238[b]	-[b]	10 ±2	DELCO[17,48]

[a] This determination is not independent of the following one.

[b] The number of events and backgrounds for the most recent analysis of this experiment are not available.

b. The D decays into an electron always have a neutrino associated with them, so for these events it is very difficult to see a peak in an invariant mass distribution. The major decays are

$$D^0 \to e^+K^-\nu, \quad e^+K^-\pi^0\nu, \quad e^+\bar{K}^0\pi\nu, \quad e^+K^{*-}\nu, \quad \text{etc.} \tag{63}$$

$$D^+ \to e^+\bar{K}^0\nu, \quad e^+K^-\pi^+\nu, \quad e^+\bar{K}^{*0}\nu, \quad \text{etc.} \tag{64}$$

The largest "Cabibbo-suppressed" decay is $D \to \pi e^+\nu$, which is expected to be a factor of $1.6\tan^2\theta$ smaller than the $D \to Ke^+\nu$ decay. The 1.6 is a phase-space factor. Since there is always at least one missing particle, it is very difficult to measure the separate branching fractions for D^0 and D^+. This would be possible at the $\psi(3772)$ for the sequence

$$e^+e^- \to D\bar{D} \begin{cases} \to eX \\ \to \text{hadrons (all particles seen)} \end{cases} \tag{65}$$

because for these events, tagged D's, the sign and branch-

ing fractions of the D decaying into hadrons are known. Using the relation (58) a count of these events for D^0 and D^+ could give us the separate branching fractions. Unfortunately, the statistics[73] collected so far at the ψ'' are not enough to allow such a method. Therefore all the semileptonic branching fractions quoted are averaged over D^+ and D^0.

c. In the experiments done so far only the electron spectrum has been measured. The K or K* decays of Eqs. (63) and (64) predict a different electron spectrum (see for example, Fig. 24). Therefore a large statistics experiment can distinguish among the two and measure each contribution separately. To calculate a branching fraction, B_e, it is necessary to calculate the acceptance (see Eq. (58)) of the apparatus, therefore an assumption has to be made on the relative importance of K and K* final states. The quoted values in Table VII depend on this assumption, although they are not too sensitive to it. The usual assumption is equal contribution from K and K*.

d. To calculate B_e one has to know σ_D, therefore the $\psi(3772)$ or the 4.03 GeV results are more reliable. At higher energies the branching fraction obtained is an average over charm particle semileptonic decays. As discussed in Section III.D, $R_{charm} = R_{D\bar{D}} + R_{F\bar{F}} + R_{B\bar{B}}$. We know $R_{D\bar{D}}$ (see Table III) at some energies, the charmed baryon contribution is at most 0.32 units of R, whereas $R_{F\bar{F}}$ is very uncertain (see Section III.B).

Table VII shows the measured branching fractions for D semileptonic decays. The LGW experiment has made two measurements, in view of (d) above. The first[73] is at the $\psi(3772)$, the second one at higher energies.[77] The electron spectra obtained in three sub-samples of the high energy data are shown in Fig. 24. The contribution of the τ heavy lepton is estimated to be 25%, assuming $B(\tau^- \to e^- \bar{\nu}_e \nu_\tau) = (18 \pm 2)\%$ and $B(\tau^- \to \nu_\tau + n_{ch} \geq 3) = (25 \pm 10)\%$.

The branching fractions measured at the $\psi(3772)$ and at higher energies agree within errors. Figure 25 shows the branching fractions measured at different energies. They are consistent with a constant value indicating that the contribution from other semileptonic decays of charmed particles is small enough not to alter B_e, or that the B_e for these other decays are not too different.

The DASP data[78] in the 4.03 GeV region are shown in Fig. 26. The branching fractions measured at 4.03 GeV and in the whole energy region are in agreement with the LGW result. Finally, the

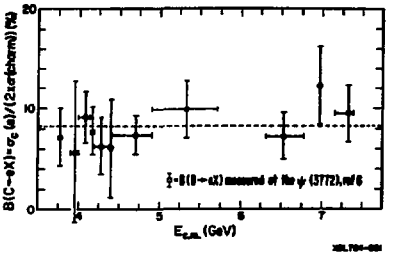

Fig. 25. The branching fraction for charmed particle decay into an electron plus additional particles as a function of energy.[77] The value at the $\psi(3772)$ is from Ref. 73. The dashed line indicates the average value of the ratio for $3.9 < E_{c.m.} < 7.4$ GeV.

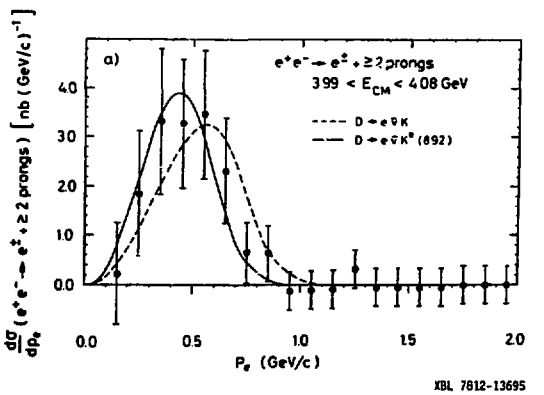

Fig. 26. The electron momentum spectrum for $D \to e\nu X$ as measured by DASP.[78]

DELCO electron spectrum[48] at the $\psi(3772)$ is shown in Fig. 27. The quoted branching fraction is somewhat larger, but not in disagreement with the other determinations.

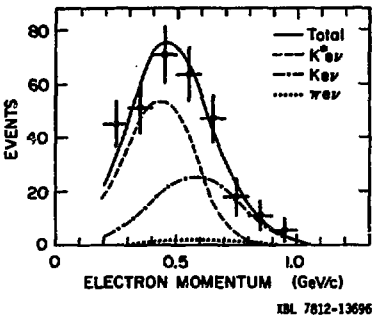

Fig. 27. The electron momentum spectrum from $D \to e\nu X$ as measured by DELCO[48] at the $\psi(3772)$. The curves shown are the result of a fit (see text).

In summary, taking the weighted average of the above results (except for DASP's result at 4.03 GeV), we obtain for the semileptonic branching fraction the value

$$B_e = (8.3 \pm 1.1)\% \qquad (66)$$

The DELCO experiment has also tried to separate the contributions to B_e from the different semileptonic decay modes. A fit to the electron spectrum shown in Fig. 27 was made to $K^*e\nu$, $Ke\nu$ and $\pi e\nu$. The fraction of $\pi e\nu$ decay was fixed whereas the other two were free to vary. The results are:

$$B(D \to Ke\nu) = (3.7 \pm 2.1)\%$$

$$B(D \to K^*e\nu) = (6.0 \pm 2.3)\%$$

$$B(D \to \pi e\nu) < 2\% \text{ (90\% CL)}$$

3. The Nonleptonic Enhancement Question. The two results most relevant to nonleptonic enhancement are given in Eqs. (59) and (66). As discussed in Section II.C.3, the semileptonic branching fraction into electrons is expected to be 20% from quark counting and as low as 3% from nonleptonic enhancement calculations.[38] The experimental result is $(8.3 \pm 1.1)\%$.

Ellis et al[38] have calculated the ratio (59); they find

$$r = \frac{\Gamma(D^+ \to \bar{K}^0\pi^+)}{\Gamma(D^0 \to K^-\pi^+)} = 4\left(1 + \frac{f_-}{2f_+}\right)^{-2} \qquad (67)$$

where f_- and f_+ are the coefficients of the terms in the Lagrangian transforming respectively as a $\underline{20}$ and as an $\underline{84}$. The coefficients f_+ and f_- from QCD calculations[38] have been found to be

$$f_- = \left[1 + \frac{33-2F}{12}\,\alpha_S(m_c)\,\ln\left(\frac{M_W^2}{M_c^2}\right)\right]^{12/(33-2F)} \qquad (68)$$

$$f_+ = \frac{1}{\sqrt{f_-}} \qquad (69)$$

where F is the number of flavors, and $\alpha_S(m_c)$ the running coupling constant at the mass of the charmed quark. Assuming $\alpha_S(m_c) = 0.7$, as obtained in studies of scaling violation in deep inelastic processes,[79] and F = 6 Cabibbo and Maiani[58] have recently calculated r and B_e. They get

$$f_- = 2.15 \qquad \text{and} \qquad f_+ = 0.68 \quad .$$

With these values then

$$r = \frac{B(D^+ \to \bar{K}^0\pi^+)}{B(D^0 \to K^-\pi^+)}\,\frac{\tau^0}{\tau^+} = 0.60 \quad . \qquad (70)$$

This value is in agreement with the measured value of (0.70 ± 0.23) τ^0/τ^+ if the two lifetimes are not too different. The effect of the $\underline{20}$ enhancement does not result in a large suppression of $D^+ \to \bar{K}^0\pi^+$ which is pure $\underline{84}$ with respect to $D^0 \to K^-\pi^+$ because the latter has a small projection in the $\underline{20}$ and a larger one in the $\underline{84}$ representation. In the limit of free quarks, one gets $f_+ = f_- = 1$ and r = 1.78.

In the same model these authors[58] have also calculated the semileptonic branching fraction. They get

$$B_e = \frac{1}{2 + 2f_+^2 + f_-^2} \sim 13\% \quad . \qquad (71)$$

In the limit of free quarks $B_e = 20\%$. Similar calculations have been done by Fakirov and Stech.[80]

In conclusion, the experimental results indicate that there is nonleptonic enhancement. The magnitude is such that it takes

the ratio (59) from r = 1.78 for no enhancement down to the observed value 0.70 and B_e from the expected 20% ($B_e = 1/(1+1+3)$) down to the observed value of 8.3%. This implies a nonleptonic enhancement of about a factor 3. This amount of observed nonleptonic enhancement can be accounted for by QCD calculations.[38,58,80]

4. D Meson Inclusive Decays. The lead-glass wall experiment has reported[71] some inclusive characteristics of D^0 and D^+ decays. This has been possible through the use of tagged D's at the $\psi(3772)$. In fact, at this energy if we know that there is a D (or $\bar{D}$) in an event, what recoils against it must be a $\bar{D}$ (or D), since there is not enough energy to produce an additional pion or a D*.

The events used in this study come from the same sample used to measure the masses and branching ratios of D mesons. We have tagged

$$141 \quad D^0 \text{ (or } \bar{D}^0) \rightarrow K^{\mp}\pi^{\pm} \tag{72a}$$

$$107 \quad D^+ \text{ (or } D^-) \rightarrow K^{\mp}\pi^{\pm}\pi^{\pm} \tag{72b}$$

by selecting the events in a narrow mass interval around the D. For D^0 we use the three highest bins in Fig. 20a; using adjacent bins the background is estimated to be 15.6%. For the D^+ sample we have taken the four highest bins in Fig. 20e. This sample has a background of non D events of 25.2%.

The simplest quantity to measure in this sample is the charged particle multiplicity. Except for background and acceptance correction this measurement requires only counting the number of observed charged particles in the system recoiling against the observed D. Since the solid angle of the detector is only 0.73 of 4π for tracking, that is, for measuring the momentum of a charged particle, a number of charged prongs escape detection. We have calculated by Monte Carlo techniques the efficiency to observe a number of charged prongs, n_{ch}, as a function of the produced number of prongs. We then use these efficiencies to unfold the "true" produced distribution from the observed one. These distributions are shown in Fig. 28. They show that 74% of the events with a D^0 have two charged prongs and 15% have four charged prongs in the decay products. For the $D^{\pm}$ we find that 37% have only one charged prong and 59% have three charged prongs in the decay products. The average unfolded multiplicites are:

$$\langle n_{ch} \rangle_{D^0} = 2.3 \pm 0.3 \tag{73a}$$

$$\langle n_{ch} \rangle_{D^+} = 2.3 \pm 0.3 \tag{73b}$$

Next we have measured the K content among these charged prongs. The charged and neutral kaons were identified as mentioned in

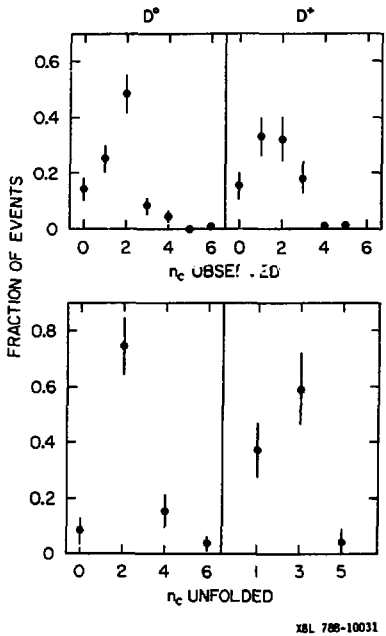

Fig. 28. Charged multiplicity distributions for D^0 and D^+ decays.[71] The data shown in the top graphs are the observed distributions; the bottom graphs have been obtained after corrections for detection efficiency.

Section III.A.1, that is, $K^\pm$ by time-of-flight (TOF) measurement, the K^0 by studying the $\pi^+\pi^-$ invariant mass. After correcting the observed $K^\pm$ content for decays in flight, TOF efficiency, tracking efficiency, and geometrical acceptance we obtain the fractions of $K^\pm$ shown in Table VIII. For K^0 we only detect K_S, so the observed events are corrected for unseen K^0 decays as well as for inefficiency in detecting K_S. Unfortunately, the statistics are very low due to the fact that the detectable $K_S \to \pi^+\pi^-$ are only one-third of all the K^0 produced. In Table VIII we note the following:

a. The total number of K/event are:

$D^0 \rightarrow K^{\pm}, K^0$ $\quad 0.92 \pm 0.28$

$D^+ \rightarrow K^{\pm}, K^0$ $\quad 0.55 \pm 0.30$

We expect at least 95% of the events to have a K, since the Cabibbo forbidden decays are ~5%. The observation is in agreement with the expectation, although the D^+ result is a little low.

b. For D^0, the statistical model of Quigg and Rosner[57] (except for a correction due to Cabibbo forbidden decays with no K's in the final state) predicts:

$D^0 \rightarrow K^-$ $\quad 0.48$

$D^0 \rightarrow \bar{K}^0$ $\quad 0.52$

to be compared with 0.34 ± 0.08 and 0.57 ± 0.26 respectively, in fair agreement within the errors.

c. For D^+, the statistical model predicts (with the same small correction mentioned above):

$D^+ \rightarrow K^-$ $\quad 0.33$

$D^+ \rightarrow K^0$ $\quad 0.67$

to be compared with the experimental values 0.10 ± 0.07 and 0.39 ± 0.29 respectively. The first value, 0.10 ± 0.07, is therefore not in good agreement with 0.33. The errors are large, therefore at this time there is no cause for alarm, but it is suggestive. An experiment with higher statistics is needed before drawing any conclusions.

TABLE VIII. Fractions of charged and neutral kaons in D^0 and D^+ decays.[71]

Mode	Events found	Background events expected	Efficiency	Branching fraction
$D^0 \rightarrow K^{\pm}X$	21.2 ± 5.1	2.4 ± 0.6	0.46	0.35 ± 0.10
$D^0 \rightarrow K^0X$	7 ± 2.6	1.1 ± 0.8	0.09	0.57 ± 0.26
$D^+ \rightarrow K^-X$	4.8 ± 2.2	1.4 ± 0.5	0.42	0.10 ± 0.07
$D^+ \rightarrow K^+X$	2.8 ± 1.7	1.1 ± 0.4	0.39	0.06 ± 0.06
$D^+ \rightarrow K^0X$	4 ± 2.0	1.3 ± 0.8	0.09	0.39 ± 0.29

Finally, we have measured the average energy going into the different particles in the final state: charged pions, kaons, photons, electrons, and muons. The average values of the energy as a fraction of the D energy are as follows:

	D^0	D^+
$\pi^\pm$	0.53 ±0.06	0.57 ±0.08
$K^\pm$	0.15 ±0.04	0.06 ±0.04
K^0	0.21 ±0.11	0.16 ±0.14
$e^\pm,\mu^\pm$	0.03 ±0.01	0.03 ±0.01
γ	0.23 ±0.10	0.20 ±0.12
Total	1.15 ±0.16	1.02 ±0.21

We expect that some energy will be carried away by the neutrinos associated with the 16% semileptonic decays. This energy will be of the same order of magnitude as that carried by $e^\pm$ and $\mu^\pm$. So we can conclude that within the errors (~20%) all the D decay energy is accounted for.

5. Cabibbo Forbidden Decays. For these decays, as discussed in Section II.C.1, the $c \to d$ transition and $u\bar{s}$ pair creation take place. We expect these rates to be suppressed by at least a $\tan^2\theta = 0.055$ factor. The SPEAR experiment SP17 has searched for these decay modes and found none.[43] Figure 29 shows the invariant mass plots for five of these possible modes; the sixth plot is $D^\pm \to K_S\pi^\pm$, not seen in that experiment, but later detected in the SP26 experiment, as discussed in Section IV.D.1 above.

The upper limits found in this experiment are expressed in terms of $\sigma \cdot B$. Since we now know σ for D^+ and D^0 at 4.03 GeV (Table III), we can express the results as a branching fraction upper limit in percent. The results are:

	Mode	Branching fraction
(a)	$D^0 \to \pi^+\pi^-$	<0.2%
(b)	$D^0 \to K^+K^-$	<0.2%
(c)	$D^+ \to K^+K^-\pi^+$	<0.6%
(d)	$D^+ \to \pi^+\pi^-\pi^+$	<0.3%
(e)	$D^+ \to K^+\pi^-\pi^+$	<0.2%

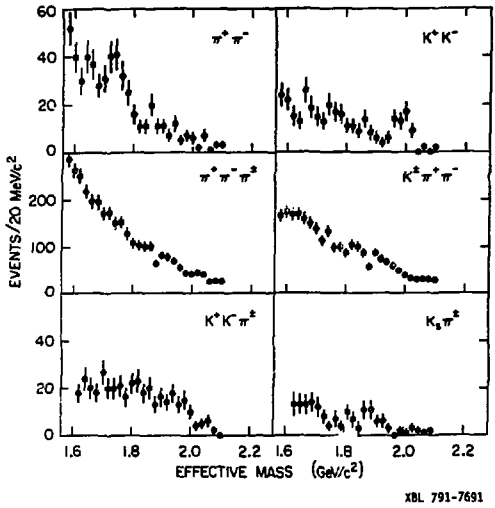

Fig. 29. Search for Cabibbo suppressed decays[43] of the D mesons [$M(D^o) = 1863$ MeV, $M(D^+) = 1868$ MeV]. The decay channel $D^\pm \to K_S\pi^\pm$ is not Cabibbo suppressed; it has been later observed by the LGW experiment[53] (see Fig. 20).

From Fig. 4a and 4e we see that, apart from kinematical factors:

$$\frac{\Gamma(D^o \to \pi^-\pi^+)}{\Gamma(D^o \to K^-\pi^+)} \sim \frac{\sin^2\theta\cos^2\theta}{\cos^4\theta} = \tan^2\theta = 0.055 \qquad (74)$$

that is, according to Eq. (15), each suppressed transition brings a $\sin\theta$ factor in the amplitude and each of the favored transitions brings a $\cos\theta$ factor. From Table VI we expect for $D^o \to \pi^-\pi^+$:

$$B(D^o \to \pi^-\pi^+) \sim (2.2 \times 0.055)\% = 0.12\%$$

smaller than the measured upper limit. For $D^o \to K^+K^-$ the same $\tan^2\theta$ factor is expected.

The D^+ decays (c) and (d) are suppressed by a $\tan^2\theta$ factor over the $D^+ \to K^-\pi^+\pi^+$ decay (see Table VI), whereas the last one,

$D^+ \to K^+\pi^-\pi^-$, is suppressed by $\tan^4\theta$. For $D^+ \to \pi^+\pi^+\pi^-$ we expect, from Table VI

$$B(D^+ \to \pi^+\pi^+\pi^-) \sim (3.9 \times 0.055)\% = 0.21\% ,$$

therefore the measured upper limits are in agreement with expectation.

6. Summary of D Decays. We can summarize the experimental results discussed in sections 1-5 as follows:

a. Only a small fraction of the hadronic decays have been measured. From Table VI,

$$\sum_{\substack{\text{measured} \\ \text{modes}}} B_i(D^0 \to \text{hadrons}) = (21.4 \pm 6.3)\%$$

$$\sum_{\substack{\text{measured} \\ \text{modes}}} B_i(D^+ \to \text{hadrons}) = (5.4 \pm 1.2)\%$$

b. The semileptonic decay branching fraction (Eq. 66) is found to be $B_e = (8.3 \pm 1.1)\%$.

c. The measured branching fraction for $D^+ \to \bar{K}^0\pi^+$ (Table VI) along with that for the semileptonic decay, indicates that there is nonleptonic enhancement in charmed particle decays, in analogy to $\Delta I = 1/2$ or octet enhancement for strange particles. The hadronic decays are enhanced by about a factor 3.

d. Inclusive D decay studies show that

i) $\langle n_{ch} \rangle = 2.3 \pm 0.3$ for D^0 and D^+.

ii) $(D^0, D^+) \to \bar{K}^0$ are more copious than decays into $K^\pm$.

iii) $B(D^+ \to K^-)$ is only $(10 \pm 7)\%$.

iv) There is no energy missing in D decays within the 20% experimental errors.

e. The Cabibbo suppressed decays are not observed; the quoted upper limits are consistent with expectation.

REFERENCES

1. J.D.Jackson, Proceedings of the 1976 Summer Institute on Particle Physics, SLAC Report SLAC-198, p.147 (1976), and LBL Report LBL-5500 (1976).

2. H.Harari, Proceedings of the 1977 Summer Institute on Particle Physics, SLAC Report SLAC-204, p.1 (1977).

3. T.Appelquist, R.M.Barnett and K.Lane, Annual Review of Nucl. and Particle Sci. 28 (1978).

4. R.F.Schwitters, Proc. 1975 Int. Symposium on Lepton Photon Interactions at High Energies, Stanford, California, p.355 (1975).

5. P.A.Rapidis et al., Phys. Rev. Lett. 39, 526 (1977).

6. T.Appelquist and H.Georgi, Phys. Rev. D8, 4000 (1973); A.Zee, Phys. Rev. D8, 4038 (1973).

7. A.De Rujula, S.L.Glashow, Phys. Rev. Lett. 34, 46 (1975).

8. G.Bonneau and F.Martin, Nucl. Phys. B27, 381 (1971); D.R.Yennie, Phys. Rev. Lett. 34, 239 (1975).

9. J.D.Jackson and D.L.Scharre, Nucl. Inst. & Meth. 128, 13 (1975).

10. S.W.Herb et al., Phys. Rev. Lett. 39, 252 (1977).

11. C.Darden et al., Phys. Lett 76B, 246 (1978); Ch.Berger et al., Phys. Lett. 76B, 243 (1978). For T see also J.Bienlein et al from the following reference.

12. J.K.Bienlein et al., Phys. Lett. 78B, 360 (1978); C.W.Darden et al., Phys. Lett. 78B, 364 (1978).

13. C.Quigg and J.L.Rosner, Phys. Lett. 72B, 462 (1978); J.L.Rosner, C.Quigg and H.B.Tacker, Phys. Lett. 74B, 350 (1978); see also C.Quigg, "New Quark Flavors," Fermilab-Conf-78/17-THY (1978), talk presented at Orbis Scientiae, 1978.

14. Particle Data Group, C.Bricman et al., Phys. Lett. 75B, 1 (1978)

15. A.M.Boyarski et al., Phys. Rev. Lett. 34, 1357 (1975).

16. V.Lüth et al., Phys. Rev. Lett. 35, 1124 (1975).

17. W.Bacino et al., Phys. Rev. Lett. 40, 671 (1977).

18. R.Brandelik et al., Phys. Lett. 76B, 361 (1978).

19. J.Siegrist et al., Phys. Rev. Lett. 36, 700 (1976).

20. G.Flügge, Proc. of the XIX Int. Conf. on High Energy Physics, 23-30 August 1978, Tokyo, Japan, and DESY Report DESY-78/55.

21. R.Van Royen and V.F.Weisskopf, Nuovo Cimento 50A, 617 (1967), and Nuovo Cimento 51A, 583 (1967).

22. T.Appelquist and H.D.Politzer, Phys. Rev. Lett. 34, 43 (1975).

23. J.E.Augustin et al., Phys. Rev. Lett. 33, 1406 (1974); Aubert et al., Phys. Rev. Lett. 33, 1404 (1974).

24. Eichten et al., Phys. Rev. Lett. 34, 369 (1975); also Phys. Rev. Lett. 36, 500 (1976); Lane et al., Phys. Rev. Lett. 37, 477 (1976); K.Gottfried, Phys. Rev. Lett. 40, 598 (1978).

25. K.Gottfried, Proc. of the 1977 Int. Symposium on Lepton and Photon Interactions at High Energy, August 1977, Hamburg (DESY, Hamburg, 1977), p.667.

26. S.Okubo, Phys. Lett. 5, 105 (1963); G.Zweig, CERN Report TH-401, 412 (1964); J.Iizuka, K.Okada, and O.Shito, Prog. Theor. Phys. 35, 1061 (1966).

27. S.L.Glashow, U.Iliopoulos and L.Maiani, Phys. Rev. D2, 1285 (1970).

28. S.Weinberg, Phys. Rev. Lett. 19, 1264 (1967); A.Salam, in Elementary Particle Physics: Relativistic Groups and Analyticity, edited by N.Svartholm (Almquist and Wiskell, Stockholm, 1968), p.367.

29. N.Cabibbo, Phys. Rev. Lett. 10, 531 (1963).

30. See the most recent review article by M.Perl, "Evidence for and properties of the τ lepton," presented at the Ben Lee Memorial Conf. on Parity Nonconservation, Weak Neutral Currents and Gauge Theories, Batavia, Illinois, October 1977, also published as SLAC-PUB-2055. See also G.Feldman, "Properties of the τ Lepton," in Neutrino-78. also published as SLAC-PUB-2138 (1978).

31. M.Kobayashi and K.Maskawa, Progr. of Theoret. Phys. 49, 652 (1973).

32. J.Ellis et al., Nucl. Phys. B131, 285 (1977).

33. L.Maiani, Phys. Lett. 62B, 186 (1976);
S.Pakvasa and H.Sugawara, Phys. Rev. D14, 305 (1976).

34. M.K.Gaillard and B.Lee, Phys. Rev. Lett. 33, 108 (1974);
G.Altarelli and L.Maiani, Phys. Lett. 52B, 351 (1974).

35. M.K.Gaillard, B.W.Lee, J.L.Rosner, Rev. Mod. Phys. 47, 277 (1975); G.Altarelli, N.Cabibbo, and L.Maiani, Nucl. Phys. B88, 285 (1975).

36. R.Kingsley et al., Phys. Rev. D11, 1919 (1975).

37. M.B.Einhorn and C.Quigg, Phys. Rev. D12, 2015 (1975).

38. J.Ellis, M.K.Gaillard and D.V.Nanopoulos, Nucl. Phys. B100, 313 (1975).

39. J.E.Augustin et al., Phys. Rev. Lett. 34, 233 (1975).

40. A.Barbaro-Galtieri et al., Phys. Rev. Lett. 39, 526 (1977); also J.Feller et al., IEEE Transactions on Nucl. Sci. NS-25, 304 (1978).

41. G.Goldhaber et al., Phys. Rev. Lett. 37, 255 (1976).

42. I.Peruzzi et al., Phys. Rev. Lett. 37, 569 (1976).

43. M.Piccolo et al., Phys. Letters 70B, 260 (1977).

44. V.Lüth et al., Phys. Lett. 70B, 120 (1977).

45. G.Goldhaber et al., Phys. Lett. 69B, 503 (1977).

46. C.Baltay et al., Phys. Rev. Lett. 41, 73 (1978)

47. Eichten et al., Phys. Rev. D17, 3090 (1978).

48. J.Kirkby, Proc. of the 1977 Int. Symposium on Lepton and Photon Interactions at High Energy, Hamburg, August 1977 (DESY, Hamburg, 1977), p.3. See also J.Kirkby, Proc. of the 1978 Summer Institute on Particle Physics, SLAC, 1978, also published as SLAC-PUB-2231 (1978).

49. A.De Rujula, H.Georgi and S.L.Glashow, Phys. Rev. Lett. 38, 317 (1977).

50. G.Knies, Proc. of the 1977 Int. Symposium on Lepton and Photon Interactions at High Energy, Hamburg, August 1977 (DESY, Hamburg, 1977), p.69.

51. I.Peruzzi et al., "Inclusive K and D production in e^+e^- annihilation," Lawrence Berkeley Laboratory Report LBL-7935, to be published (1978).

52. P.A.Rapidis et al., "Inclusive production of D mesons in e^+e^- annihilation at 7 GeV," to be published (1978).

53. I.Peruzzi et al., Phys. Rev. Lett. 39, 1301 (1977).

54. R.Brandelik et al., Phys. Lett. 70B, 132 (1977). See also S.Yamada, Proceedings of the 1977 Int. Symposium on Lepton and Photon Interactions at High Energy, Hamburg, August 1977, (DESY, Hamburg, 1977), p.47.

55. R.Brandelik et al., "Production characteristics of the F meson," DESY Report (October 1978).

56. D.Lüke, Proceedings of the 1977 Meeting of the Division of Particle and Fields, Argonne 1977, p.441 (1977).

57. C.Quigg and J.L.Rosner, Phys. Rev. D17, 239 (1978).

58. N.Cabibbo and L.Maiani, Phys. Rev. Lett. 73B, 418 (1978).

59. E.G.Cazzoli et al., Phys. Rev. Lett. 34, 1125 (1975).

60. B.Knapp et al., Phys. Rev. Lett. 37, 882 (1976).

61. M.Piccolo et al., Phys. Rev. Lett. 39, 1503 (1977).

62. A.De Rujula, H.Georgi and S.L.Glashow, Phys. Rev. D12, 147 (1975).

63. J.Wiss et al., Phys. Rev. Lett. 37, 1531 (1976); H.K.Nguyen et al., Phys. Rev. Lett. 39, 262 (1977).

64. P.B.Wilson et al., Stanford Linear Accelerator Report SLAC-PUB-1894 (1977).

65. G.J.Feldman et al., Phys. Rev. Lett. 38, 1313 (1977).

66. A.De Rujula, H.Georgi and S.Glashow, Phys. Rev. D12, 147 (1975).

67. K.Lane and S.Weinberg, Phys. Rev. Lett. 37, 717 (1976).

68. See e.g., A.De Rujula, H.Georgi and S.L.Glashow, Phys. Rev. Lett. 35, 69 (1975); R.Kingsley, Phys. Lett. 63B, 329 (1976).

69. S.L.Glashow and S.Weinberg, Phys. Rev. D15, 1958 (1977); E.A.Paschos, Phys. Rev. D15, 1966 (1977).

70. See for example, S.Ono, Phys. Rev. Lett. 37, 655 (1976).

71. V.Vuillemin et al., Phys. Rev. Lett. 41, 1149 (1978).

72. D.L.Scharre et al., Phys. Rev. Lett. 40, 74 (1978).

73. J.M.Feller et al., Phys. Rev. Lett. 40, 274 (1978).

74. A.Barbaro-Galtieri, Proc. of the 1977 Int. Symposium on Lepton and Photon Interactions at High Energy, Hamburg, August 1977 (DESY, Hamburg, 1977), p.21.

75. J.E.Wiss et al., Phys. Rev. Lett. 37, 1531 (1976).

76. W.Braunschweig et al., Phys. Lett. 63B, 471 (1976).

77. J.M.Feller et al., Phys. Rev. Lett. 40, 1677 (1978).

78. R.Brandelik et al., Phys. Lett. 70B, 387 (1978). See updated values of the branching fraction in B.H.Wiik and G.Wolf, "A review of e^+e^- interactions," DESY Report DESY-78/23 (1978).

79. A.De Rujula, H.Georgi and D.Politzer, Ann. Phys. 103, 315 (1977).

80. D.Fakirov and B.Stech, Nucl. Phys. B133, 315 (1978).

81. J.D.Jackson, C.Quigg and J.L.Rosner, Proc. of the XIX Int. Conf. on High Energy Physics, 23-30 August 1978, Tokyo, Japan and LBL Report LBL-7977.

82. J.D.Jackson, Proc. of the European Conf. on Particle Physics, July 1977, Budapest, Hungary, Vol. 1, p.603 (1977).

83. T.Ferguson et al., SLAC Report SLAC-2081r and UCLA Report UCLA-1116r, to be published in Phys. Lett. (1979).

84. R. E. Shrock and L.-L. Wang, Phys. Rev. Lett. 41, 1692 (1978).

ACKNOWLEDGMENTS

This work was supported by the Physics Division of the U.S. Dept. of Energy under contract No. W-7405-ENG-48.